2011

The Use of Targeted Charge-Reversal Nanoparticles (TCRNS) To Investigate Nuclear Delivery of Fluorescent Agents to Cancer Cells: Implications for Novel Prostate and Breast Cancer Therapy

Mario Dance
Virginia Commonwealth University

The Use of Targeted Charge-Reversal Nanoparticles (TCRNS) To Investigate Nuclear Delivery of Fluorescent Agents to Cancer Cells: Implications for Novel Prostate and Breast Cancer Therapy.

A thesis submitted in partial fulfillment of the requirements for the degree of Master of Science in Pharmacology and Toxicology, at Virginia Commonwealth University.

by

Mario Edwardo Dance

BS from Virginia Polytechnic Institute and State University 1986

DVM from Virginia-Maryland Regional College of Veterinary Medicine 1990

Director: Shawn E. Holt, Ph.D. Pharmacology/Toxicology

Virginia Commonwealth University

Richmond, Virginia

September 2011

Acknowledgements

I would like to thank the following people for all of their help and support in this graduate work. First I thank my advisor, Dr. Shawn Holt, for his willingness to invest in a novel graduate project and a novel graduate student experience. I thank my PhD committee members Dr. Joy Ware, Dr. Lynne Elmore, Dr. Andrew Yeudall, and Dr. Jolene Windle for their good faith efforts to help me to make the most out of a challenging turn of events. I would like to thank Dr. Stephen Sawyer for his help in transitioning to a Master's degree. I thank Amanda Richardson and the members of the Holt-Elmore lab Dr. Patrick Sachs, Min Zhou, and Xu Wang for their patience in responding to the million and one questions that I had along the way. I thank the generous staff of DAR for their investment of time and resources and for their patience in working with a veterinarian who had to reduce his clinical duties to accomplish this work. I parents for their patience and I thank my housemates for putting up with endless complaining and for being better than brothers to me. And finally I thank God for the grace and strength to get through it all.

Science can purify religion from error and superstition; religion can purify science from idolatry and false absolutes. Each can draw the other into a wider world, a world in which both can flourish. ***Pope John Paul II***

TABLE OF CONTENTS

List of Abbreviations

ABAM	Antibiotic/Antimycotic Solution
ASC	Adipose Derived Stem Cells
BJF	BJ foreskin fibroblast
BSA	Bovine Serum Albumin
DAPI	4',6-diamino-2-phenylindole
DiR	Dimethyl Indole Red
DMEM	Dulbecco's Modified Eagle's Medium
DOX	Doxorubicin
FA	Folic Acid
FACS	Fluorescence-Activated Cell Sorting
FBS	Fetal Bovine Serum
FR	Folate Receptor
GFP	Green Fluorescent Protein
GPI	Glycosyl-phosphatidylinositol
IACUC	Institutional Animal Care and Use Committee
IF	Immunofluorescence
M12	Tumorigenic sublines of human prostate epithelial cells previously immortalized by transfection with the SV40T antigen gene developed by sequential passage in male athymic nude mice.
M12-luc	M12 prostate cell line that was tranfected to express luciferase using Lipofectamine™ and a PGL-3 plasmid vector.

MDA-231	MDA-MB-231 a highly metastatic and osteolytic human breast cancer cell line obtained from a patient in 1973 at M. D. Anderson Cancer Center.
5-MTHF	5-methyltetrahydrofolate
NP-40	Tergitol-type nonyl phenoxypolyethoxylethanol
NP	Nanoparticle
NR	Nile Red
PBG	Cold Water Fish Gelatin with BSA dissolved in PBS
PBS	Phosphate Buffered Saline
PCL	Polycaprolactone
PD	Population Doublings
PEI	Polyethyleneimine
RFC	Reduced Folate Carrier
RIPA	Radio-Immunoprecipitation Assay
ROI	Region of Interest
SC	Subcutaneous
SCP	SCP28-S4-Tet-Duo Breast Cancer Cells
SDS-PAGE	Sodium Dodecyl Sulfate Polyacrylamide Gel
TCRN	Targeted Charge-Reversal Nanoparticle
XIT	Xenogen® Imaging Technology

List of Figures and Tables

ABSTRACT

THE USE OF TARGETED CHARGE-REVERSAL NANOPARTICLES TO INVESTIGATE NUCLEAR DELIVERY OF FLUORESCENT AGENTS TO CANCER CELLS: IMPLICATIONS FOR NOVEL PROSTATE AND BREAST CANCER THERAPY

By Mario Dance DVM

A thesis submitted in partial fulfillment of the requirements for the degree of Master of Science in Pharmacology and Toxicology at Virginia Commonwealth University 2011.

Major Director: Shawn E. Holt, Ph.D., Pharmacology/Toxicology

Nanotechnology has recently emerged as a strong contributor toward research efforts to develop targeted systems of drug delivery in cancer therapy. Our work investigates the therapeutic potential of Targeted Charge-Reversal Nanoparticles (TCRNs), a novel nanoparticle with *in vitro* evidence of nuclear drug delivery. Using M12 prostate cancer cells, MDA-MB-231 breast cancer cells, and modified derivatives of these cell lines, we investigated the ability of Folic Acid-tagged TCRNs to deliver Nile Red and Dimethyl Indole Redfluorescent (DiR) fluorescent dyes to the nucleus of cells using confocal microscopy and *in vivo* biphontonic imaging using Xenogen® Technology. Confocal imaging with the SCP28 derivative of MDA-MB-231 cells shows nuclear association of the TCRNs over time, although specific nuclear deposition was unclear. Biophotonic imaging with M12 and SCP28 xenograft tumors in athymic nude mice shows retention of TCRNs in animals out to 7 days with minimal localization of TCRNs to tumor tissues. Our findings suggest that further characterization and manipulation of both the cells and the nanoparticle is necessary in order to make definitive claims regarding the TCRN's ability to deliver fluorescent dyes, and eventually therapeutic compounds, to the nucleus of cells.

Chapter 1

Introduction

Cancer Therapy

The Centers for Disease Control report that cancer claims the lives of more than half a million Americans every year. Cancer is the second leading cause of death in the United States, exceeded only by heart disease. Of the various cancers detected in the USA, cancers of the breast rank highest in women and cancers of the prostate rank highest in men (1). The search for therapies for all forms of cancer continues with limited success. Traditional approaches in cancer treatment have focused on killing all actively dividing cells whether or not they were cancer or normal cells. Further advances have resulted in developing therapies that target destruction of the cancer while minimizing damage to healthy tissues and cells. Historically, drug and radiation cancer therapies predominate but advances are frustrated by significant patient toxicities and side effects due to lack of specificity (2). Various attempts have been made to address these problems with variable success, indicating a need to investigate novel systems for drug delivery that can circumvent adverse patient reactions while retaining high levels of drug toxicity that target the rapidly dividing cancer cells.

Nanotechnology

Engineers refer to Nanoparticles (NPs) as structures that are measured in the nanometer range (generally less than 100 nm in diameter) (3). In recent years, the field of Nanotechnology has produced many advances that use NPs with applications in medicine, including aids in

diagnostics, biomimetic and biohybrid systems, and therapeutics that employ novel drug delivery techniques. Recently, many promising nanotherapeutics for drug delivery have been developed, many of which have successfully delivered therapeutic agents *in vitro* (3-5). These nanostructures can be loosely categorized based on their chemistry and structure. Liposomes, for example, are small vesicular structures generally composed of a phospholipid bi-layer with an aqueous core. This structural arrangement confers properties to the NP that are similar to those of cell membranes. Liposomes can be loaded with drugs and used to deliver compounds to treat cancer and other diseases. Similar to liposomes are polymeric micelles, which make use of organic polymeric structures usually in a uni-layer, spherical configuration. Fullerenes and nanotubules are structurally and functionally similar hollow structures that can also potentially be used to carry drugs, although they are more rigid and are typically composed of carbon, metal (gold or silver), or silicon. Quantum dots are smaller, charged, solid spheres that are typically used for bioimaging, for carrying drugs that can be tagged to their surface, and for carrying highly charged materials. Examples of these nanoparticle structures are shown in Figure 1. More elaborate nanotechnologies are being developed that modify and use these basic structures in various combinations (6-7).

The use of NPs in medicine, while promising, is not without significant challenges. Previous studies show that depending on the starting material, the NP is prone to elimination via the body's natural immune system primarily through phagocytosis by macrophages (8-10). Additionally, once NPs enter a living organism, they must fight against an array of natural host defenses and changes in the microenvironment that can result in their elimination or in the premature release of their therapeutic contents, ultimately leading to the same toxic side effects that arise from therapeutic agents delivered by more conventional means. Assuming that NP-

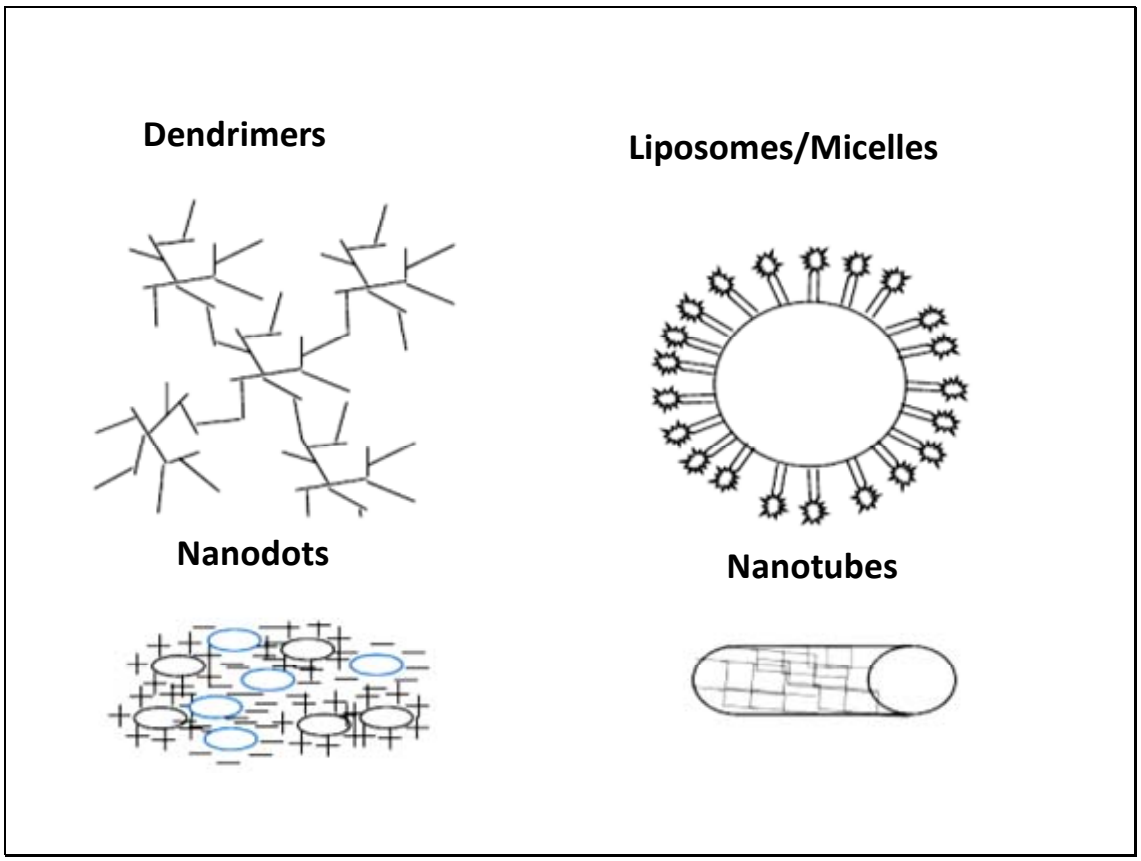

Figure 1: Basic Nanoparticle Structures. Nanoparticles have been designed using these basic structures alone or in combination with each other. Shown above are the regularly branched Dendrimer structure, the spherical Liposomes/Micelle structure, the solid and charged Nanodot structure, and the hollow Nanotubule/Fullerene structure.

carrying drugs are able to survive the host's immune system, it then needs to retain and deliver the therapeutic agent to the targeted tissue or body system. Through all of these challenges, the NPs must circumvent obstacles related to water or fat solubility, membrane permeability, pH alterations, cell surface receptor interactions, and charge limitations, all of which affect the NP's ability to retain the effectiveness of its therapeutic agent (3, 7). The NP that survives host defenses, that retains its therapeutic agents, and that selectively targets cancer cells for delivery of their contents will be a powerful asset in cancer therapy. Such a targeted NP would theoretically reduce patient toxicity by reducing the dosage of the therapeutic agent while, at the same time, still concentrating the agent and its effect at the site of the cancer.

Despite these challenges, nanotechnology is still a promising alternative to conventional drug delivery. Studies with liposomes, polymeric micelles and nanotubules show results indicating successful delivery of different therapeutic agents to cells especially under *in vitro* conditions (3-4, 11-12). While some NP-mediated therapies have begun to enter clinical trials (6, 13-15), most NPs have shown very limited success for drug delivery *in vivo* due, in part, to the aforementioned fact that once the NPs are introduced into a living organism, they are subject to natural host defenses and microenvironment changes that result in their elimination or in a premature release of their therapeutic contents (3, 16). If NPs could target not only the cell but the nucleus of the cell, this could potentially magnify a drug's therapeutic potential exponentially. The focus of our study was to investigate the therapeutic potential of the Targeted Charge-Reversal Nanoparticles (TCRNs) to deliver agents to the nucleus of breast and prostate cancer cells.

Targeted Charge-Reversal Nanoparticles

TCRNs are unique NPs, and studies suggest they can successfully deliver chemotherapeutic agents to the nucleus of human ovarian carcinoma cells (SKOV-3) *in vitro* (11, 17). The TCRNs are based on a polymeric micellar system that has been developed by Dr. Youqing Shen at the University of Wyoming. Dr. Shen is a noted polymer chemist with significant experience in generating NPs for specific delivery of compounds to the nucleus of eukaryotic cells. The NP used for our experiments is constructed using 3 different polymers that combine to form a pH-responsive structure, which has the potential to deliver drug past the cytoplasm into the nucleus of the cell. The NP is made up of a negative-to-positive charge-reversal polyethyleneimine (PEI) polymer outer layer that responds to pH changes, which is only triggered at specific locations related to the cell. The TCRNs reportedly undergo a conformational change during exposure to the extracellular acidic environment (pH<7), which is often found around inflamed or neoplastic tissues and within the acidic lysosomal environment (pH 4–5) during cell entry (11, 17). In general, negatively charged polymers have little interaction with blood components, so the PEI polymer has been used extensively *in vivo* for this purpose (3, 18). There is a second hydrophobic polymer, polycaprolactone (PCL), joined with the PEI that together combines to stimulate the formation of the micellar system responsive to changes in pH. Previous experiments (19) showed that the micelles formed by this polymer combination, when linked with a FA moiety (the third component of the terpolymer), can navigate the pH shifts in blood, tumor, and intracellular liposomal environments in such a way as to carry drug to the nucleus of the cell (Figure 2). These *in vitro* results found that TCRNs carrying doxorubicin (DOX) are more effective at killing SKOV-3 cancer cells than free DOX alone (11). If this experiment can be duplicated using other cell lines while carrying different

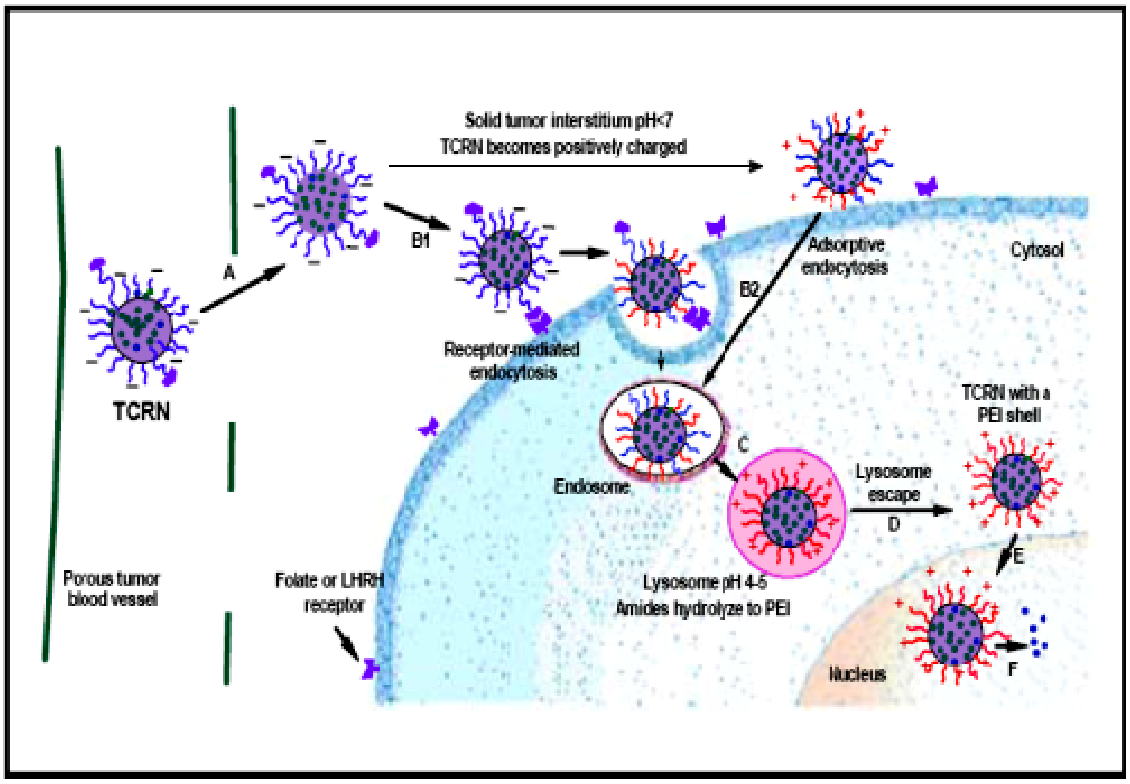

Figure 2: Schematic representation of the movement of TCRNs into the cell. TCRNs move out of vascular circulation into the tumor microenvironment where they undergo pH and charge alterations that permit them to move into the cell to deposit their contents into the nucleus. *Image used with permission (Dr. Youqin Shen).*

therapeutic agents in both *in vitro* and *in vivo* systems, then this TCRN system could have major therapeutic implications for many cancer types.

For our studies, TCRNs were conjugated with folic acid (FA) to employ the folate receptor (FR) as a target for attachment to and entry into the cell. FAs (also known as pteroylglutamic acid, vitamin B9, B_c folacin, and folate) are essential cofactors for many biochemical reactions involving one-carbon metabolism, including purine and thymidine synthesis, remethylation of homocysteine to methionine, and conversion of serine to glycine. The role of this vitamin in the production of precursors for DNA synthesis and repair makes it essential for proliferating cells (20-21). The high affinity FR is a membrane-associated glycoprotein that is preferentially expressed in cancers of epithelial origin (20, 22-23), which makes it an ideal candidate for many novel targeted drug therapies and is the focus of many NP driven studies (4, 21, 24).

FAs are used in many cellular processes, but the hydrophilic and anionic nature of FAs, at physiologic pH, impedes their passive diffusion through the plasma membrane. Therefore, most cells acquire the FA needed for normal cell processes primarily by two separate mechanisms. One involves a transmembrane transporter, known as the reduced folate carrier (RFC), named because of its inability to bind FA, the nonphysiologic, oxidized form of the vitamin. This ubiquitously expressed RFC protein has a high affinity for 5-methyltetrahydrofolate (5-MTHF) (K_d 3– 4.0μmol/L), which is the predominant FA formulation found in serum although it has a much lower affinity for FA (K_d 5 100–200μmol/L). The RFC is also present throughout development and in normal adult tissues, despite significant variability in its expression levels among tissue types (25-26).

The other primary FA uptake system uses a glycosyl-phosphatidylinositol (GPI)-anchored protein known as the FR that transports FAs into the cytosol via fluid-phase endocytosis. The physiologic function of the FR in adult tissues has largely remained a mystery since, in addition to its narrow tissue distribution, the FR is predominantly expressed on the apical (luminal) surface of polarized epithelial cells, where it is not in contact with circulating FA. This FR binds its ligands with very high affinity, having a K_d of 0.4nmol/L for FA and 3nmol/L for 5-MTHF (25-27).

There are four isoforms of the FR (FRs –α, –β, –γ and –δ) that vary somewhat in sequence, ligand preference, and tissue distribution, such that only one isoform, designated FR-α, is thought to be physiologically relevant with respect to the targeting of solid tumors in therapy because of its tendency to be over expressed in many tumor types (20). FR-α and FR-β are membrane-associated proteins, whereas FR- γ lacks the signal for GPI-anchor attachment and is constitutively secreted (27-28). FR-β has some clinical relevance as it is expressed in later stages of normal myelopoiesis and in placenta, spleen, and thymus. FR-β is also expressed in leukemic blasts in chronic and acute myelogenous leukemia (27). Because we focused primarily on the function of the FR-α in our cells, unless stated otherwise, all references to the FR will signify the more physiologically relevant FR-α.

As stated, the FR is expressed at the luminal surface of polarized epithelial cells of normal adult tissues including proximal kidney tubules, type I and II pneumocytes in the lungs, choroid plexus, ovary, fallopian tube, uterus, epididymis, submandibular and bronchial salivary glands, and trophoblasts in placenta, as well as the basolateral membrane of retinal pigment epithelial cells (25). Several malignant tumors are known to overexpress FR, including non-mucinous adenocarcinomas of the ovary, uterus and cervix, testicular choriocarcinoma,

ependymal brain tumors, malignant pleural mesothelioma, and nonfunctioning pituitary adenocarcinoma. In other malignant types of cancer such as breast, colon, and renal cancers, FR over-expression is less frequent but still common enough to be exploited (27-28) While virtually every potential drug target protein in malignant cells is also expressed in at least a few critical normal tissues, this differential anatomic distribution of FR renders it generally inaccessible directly through the blood stream in normal tissues, making it a preferred target to effectively address the problem of tumor specificity. Moreover, the receptor specifically and tightly binds a small water soluble molecule, FA, that is amenable to chemical conjugation of small and large drug molecules or nanoparticles without disruption of its binding properties (18, 27).

In vitro studies suggest that the TCRN NPs attach to cells using the FR and then are later brought into the cell via endocytosis (Figure 2) (11, 17). The proposed mechanism for this attachment hinges on the metabolic and inflammatory processes that occur near the actively growing tumor and the increased vascular permeability in the tumor microenvironment. It is hypothesized that when the blood borne negatively charged TCRN carrying drug circulates near this weakly acidic microenvironment, it extravasates, becomes positively charged, and is internalized within the cell either by receptor-mediated endocytosis or by adsorptive endocytosis (endosome). Once the NP gains entry into the cell by either mechanism, it is transferred to the strongly acidic lysosome where the PEI/amide outer layer is hydrolyzed into PEI, the NP undergoes a conformational change, and the modified TCRN is then released from the lysosome to subsequently enter the nucleus for drug delivery (11, 17).

In this study, we aim to verify this claim in additional cell lines and to confirm that TCRNs are actually able to target and deliver fluorescent dyes to breast and prostate cancer cells in an *in vitro* environment. Further, we hope to show that these TCRNs are also uniquely able to

deliver fluorescent dyes, not simply to the cytoplasm, but to the nucleus of breast and prostate cancer cells. Our central assertion is that TCRN's are capable of delivering fluorescent agents to the nucleus of carcinoma cells. TCRN delivery can be manipulated by exploiting pH changes in the microenvironment of the cell and by utilizing the cell surface FR as a mechanism for cellular delivery in an *in vivo* and an *in vitro* environment.

Fluorescent Imaging

This study makes use of several imaging technologies, all of which are based on the same fundamental principles that govern our ability to see light. Photons that strike objects are reflected or absorbed, creating a signal that registers on an image transducer. The vertebrate retina, which absorbs and transduces photon signals to the brain producing an image, is the simplest example of this principle. Engineers take this basic principle and translate it into technology that permits visualization of things that are not visible with the unaided eye. We can visualize internal organs macroscopically using technologies that manipulate sound (ultrasound imaging), X-ray radiation (radiographic imaging), and ionizing radiation (magnetic resonance imaging). On a microscopic level, manipulating electrons and lasers helps us to magnify images that are beyond the ability of ordinary light microscopes. All of these technologies can be further enhanced using contrasting agents that further amplify or modify the signal being recorded. Radiography, for example, uses barium or iodine contrast agents to improve visualization of organs, while microscopy uses fluorescent agents to improve visualization of cellular structures and organelles (29-30).

In our study, we use optical fluorescent imaging technology and Xenogen Imaging Technology (XIT) to confirm the ability of the TCRNs to deliver their contents to the cell.

Confocal microscopy is an advanced form of light microscopy, useful for viewing fluorescently labeled cellular structures. An object of interest is labeled or tagged with a fluorophore that, when illuminated with light of a specific wavelength, will absorb the light and emit a signal at another longer wavelength that is detected by the optical imaging device and transmitted as color. Confocal microscopy uses this same principle with light generated by lasers of different wavelengths that scan the sample in a more focused manner. The illumination is confined to a diffraction-limited spot in the specimen and the detection is similarly confined. All of this produces an 'optical sectioning' effect, in which the glare from out-of-focus regions is almost completely eliminated and the image sharpened (31).

Bioluminescent *in vivo* imaging using XIT, also known as biophotonics, employs similar principles to image macroscopic objects in real time. This *in vivo* imaging is a noninvasive technique using bioluminescent and fluorescent endogenous reporters or exogenous probes to monitor molecular and biological processes. In the simplest terms, it is a device with a sensitive camera that measures light produced by biological or chemical moieties. The object being imaged is placed on the sample stage where the fluorescent signal passes through the animal to the lens and filters and, ultimately, to the camera. The light is detected by the sensitive camera and superimposed over a normal camera image of the animal/object (Figure 3). It is a non-invasive time/space visualization of biological processes inside of a live animal, relying on light producing optical reporters such as luciferase, fluorescent proteins, fluorescent dyes and conjugates. Genes encoding luciferase and fluorescent proteins can be engineered into cells (e.g., cancer cell lines and infectious disease agents) and into animals (transgenic mice and rats), which enables them to produce light that can then be visualized through the tissues of a live animal using specialized Xenogen imaging equipment and software (30, 32). Most commonly,

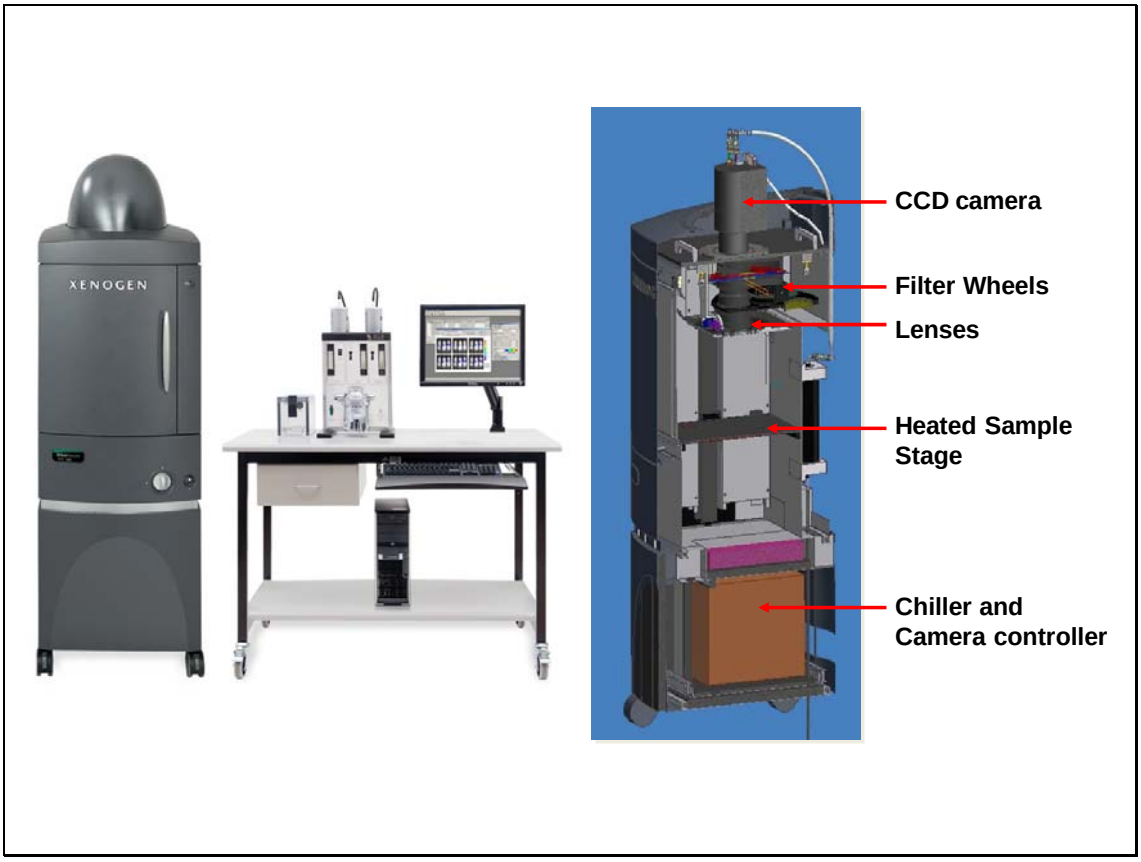

Figure 3: IVIS® Spectrum Imaging System. On the left is the Xenogen machine positioned next to its anesthesia vaporizer and computer for image analysis. On the right is a schematic of the machine's internal imaging components. *Image is courtesy of Caliper Life Sciences.*

the imaging device measures luminescent signals that are produced when natural biological substances, typically luciferin or green fluorescent protein (GFP), are injected into or otherwise expressed in animals and excited by a substrate-driven enzymatic processes to produce light at different wavelengths. Similarly, the device can be used with fluorophores or fluorescent reporters that come in a wider variety of forms: expressed proteins, dyes, microspheres, and NPs. Visualization of fluorescent reporters does not require the administration of a substrate and can be used in both live and fixed cells/tissues (29). This highly sensitive dual bioluminescence and fluorescence imaging systems has the advantage of allowing significantly fewer animals to be used due to the fact that the entire process is non-invasive. Additionally, this technology allows us to follow the development of tumors and to monitor the intensity of any fluorescent signal present in the tumor over time in the live animal. The final image produced by XIT is a composite image composed of a photographic image of the object superimposed over a luminescent image with intensity of luminescence represented by gradations in color (Figure 4).

In this study, we aimed to verify the nuclear delivery claims of the TCRNs by integrating a fluorescent dye into the core of the NP and working to show that this dye is being deposited into our cells. Our goal was to show that the dye is ultimately deposited in the nucleus of cancer cells, suggesting that the TCRNs will function similarly when carrying chemotherapeutic agents. In so doing, we expected to demonstrate by proof of principle the potential use of TCRNs for delivery of therapeutic agents into cells, further suggesting that TCRNs can be used to reduce the dosage of chemotherapeutic agents that often target the DNA machinery in the nucleus and are highly toxic to patients.

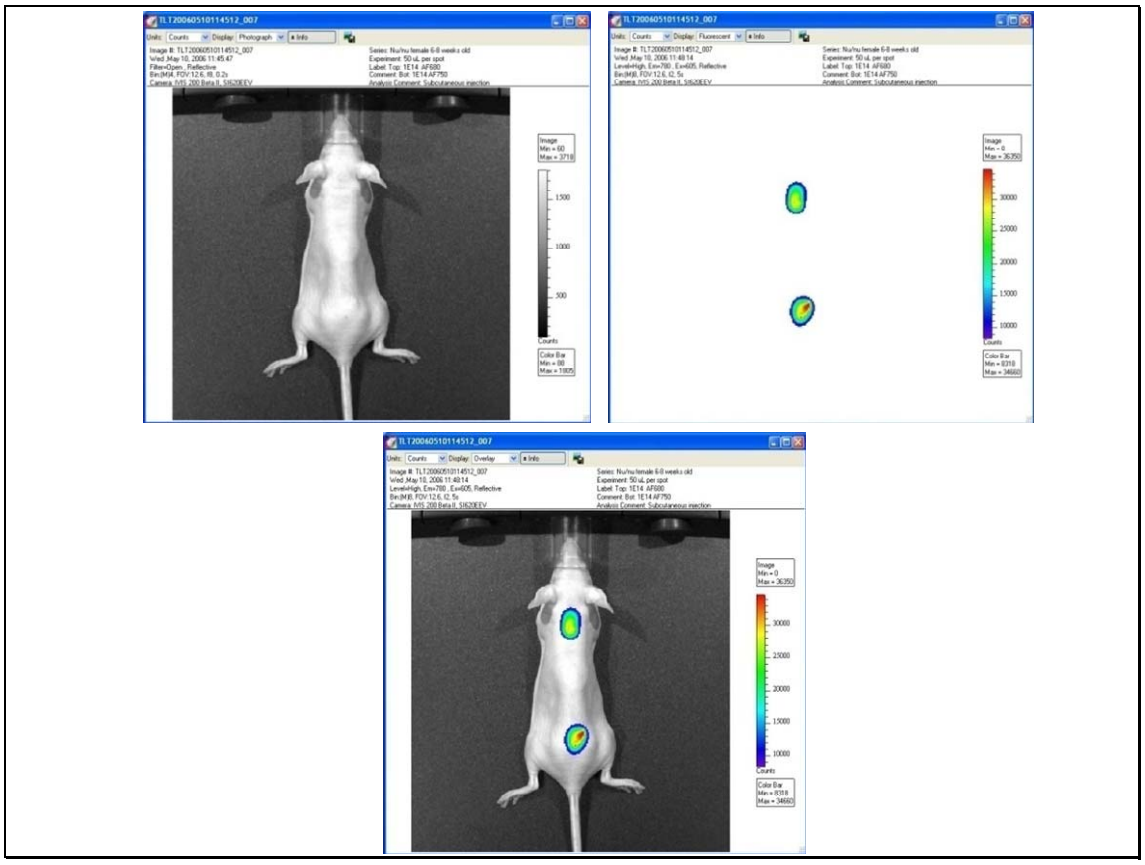

Figure 4: Construction of the Xenogen Image. Standard images are composed of two superimposed images: Photographic image + Luminescent image = Overlay image. These are screen shot images of what is seen when measurements are taken using the Xenogen imager. *Image is courtesy of Caliper Life Sciences.*

The overall hypothesis and specific aims are as follows:

Hypothesis: We propose that TCRNs carrying fluorescent dyes will selectively deposit their contents into the cytoplasm and the nucleus of carcinoma cells using the FA/FR interaction producing changes in fluorescent signaling as observed by *in vitro* and *in vivo* assays.

Specific Aim: To characterize and verify the FR profile of our prostate and breast cancer cell lines in order to 1) demonstrate TCRN dye delivery and 2) correlate TCRN function with the FR using differences in fluorescent signaling within the cytoplasm and the nucleus of tumor cells.

Chapter 2

Materials and Methods

Cell Lines and Culturing: Several cell lines were used for this study: M12 prostate cancer cells; M12-luc cells, which are prostate cancer cells stably transfected to express luciferase; MDA-MB-231 breast cancer cells; SCP28-S4-Tet-Duo breast cancer cells, which are also engineered to express luciferase; BJ foreskin fibroblast (BJF); and adipose derived stem cells (ASC). BJ fibroblasts were grown in high glucose Dulbecco's modified Eagle's medium (DMEM; Invitrogen) supplemented with 10% cosmic calf serum (Hyclone) and 1% Antibiotic/Antimycotic Solution (ABAM; Sigma-Aldrich). ASC-8 at PD10 were previously isolated in our laboratory from a lipoaspirate obtained from the VCU Surgery Department in accordance with VCU IRB procedures for medical waste. ASC-8 cells were grown in low glucose DMEM supplemented with 10% fetal bovine serum (FBS; Invitrogen) and 1% ABAM. Both the M12 and the M12-luc cells were cultured in Roswell Park Memorial Institute (RPMI; Invitrogen) medium supplemented with 0.03mg/ml gentamicin+ 0.3mg/ ml L-glutamine + 0.1% ITS (Insulin/Transferrin/Selenium; VWR Radnor, PA) + 5% FBS. MDA-231 and SCP28-S4-Tet-Duo breast cancer cells were cultured in RPMI medium supplemented with 0.03mg/ml gentamicin + 0.3mg/ml L-glutamine + 5% FBS.

The principle cell lines used for all of the experiments are the M12 and M12-luc prostate cancer cell line, and the MDA-MB-231 and SCP28 breast cancer cell lines. The M12 cell line is a tumorigenic, metastatic subline of human prostate epithelial cells previously immortalized by transfection with the SV40T antigen gene, developed by Dr. Joy Ware by sequential passage of

the cells in male athymic nude mice (33). The SCP is a single cell-derived subline of MDA-MB-231 that is highly osteolytic and metastatic, but it is also engineered for bioluminescent imaging. This cell line was engineered to express Renilla luciferase under a constitutively active cytomegalovirus promoter for quantitative measurement of metastatic tumor burden *in vivo* through noninvasive bioluminescence imaging using coelanterazine as the substrate. It also expresses firefly luciferase using D-luciferin as the substrate (34).

Western Blot Analysis: To confirm the presence of the FR in M12, M12-luc, MDA-231, BJF, and ASC cells, we performed Western analysis for FR and β-actin (as an internal control). Cells were trypsinized and then lysed with Radio-Immunoprecipitation Assay (RIPA) buffer supplemented with protease inhibitor (Sigma) for 30mins on ice. Whole cell lysates were prepared from each of these cell lines and subjected to five 20 second pulse intervals of sonication at power level 2 using a Misonix 3000 sonicator in order to shear the genomic DNA prior to gel electrophoresis. The samples were placed on ice between treatment intervals. After sonication, lysates were clarified by centrifugation at 11,000 x g for 20mins. The resulting supernatant was collected and analyzed for total protein content using a Biorad Protein Assay kit and a spectrophotometer. Protein samples were treated with non-reducing 4x sample buffer (4% SDS, 20% glycerol, 0.004% bromophenol blue, 0.125M Tris HCl, at pH 6.8) at 85°C for 10mins and then loaded (25μg total protein per sample) on a 10% sodium dodecyl sulfate polyacrylamide gel (SDS-PAGE) followed by electrophoresis for approximately 1.5 hours. Following SDS-PAGE, the gel was transferred to nitrocellulose membrane by electroblotting at 100 volts for approximately 1 hour. The membrane was blocked using 5% non-fat milk for 1 hour at room temperature, followed by multiple washes with PBS+1% Tween-20 (PBS-T). The

blot was incubated with primary antibodies (anti-folate, at 5µg/ml; Enzo Life Sciences; anti-β-actin at 1µg/ml; Sigma) for 1 hour at room temperature, followed by multiple PBS-T washes. Secondary antibody (goat anti-mouse conjugated to horseradish peroxidase, at 1µg/ml dilution; #172-1011 BIO-RAD, Hercules CA) was used to probe the blot for 1 hour at room temperature, followed by extensive washing with PBS-T. Pierce SuperSignal (luminol and peroxide solutions) was used for detection, and the blot was exposed to Kodak OMAT film and developed. We used this non-reducing protocol because the FR is a complex cell surface protein whose conformation is very sensitive to reducing reagents, and our particular antibody was not able to recognize the FR protein after it had been treated with a reducing protocol. We needed to adjust the normal Western assay to eliminate exposure to reducing agents so that our primary antibody could recognize the protein.

Fluorescence-Activated Cell Sorting (FACS) Analysis: To quantify and further characterize the presence of the FR on the cell surface of the M12, M12-luc, MDA and SCP cell lines, we used FACS analysis. The cells were cultured in cell-specific media and then harvested with 0.25% (w/v) trypsin-0.1% (w/v) EDTA solution and counted, adding approximately $1x10^6$ cells to sample tubes. The cells were incubated in FACS buffer (PBS + 1% FBS) at room temperature for 15mins and then on ice for 10mins. Following this stabilization period at room temperature to allow cell surface proteins to recover from trypsin treatment, the cell suspension was treated with primary mouse monoclonal antibody (anti-folate, at 5µg/ml; Enzo Life Sciences, Plymouth Meeting, PA) and incubated for 30mins on ice rocking gently. Cells were washed 3 times with FACS buffer and then treated with secondary antibody (goat anti-mouse IgG conjugated to Alexa 488 at 1µg/ml; A11029 Invitrogen) on ice rocking gently. Cells were washed again 3

times in FACS buffer and then counted in BD FACSCanto II Flow Cytometer using DIVA software for signal analysis.

Fluorescent Microscopy: To assess the relative expression level of the folic acid receptor *in vitro*, $1x10^4$ cells were seeded and were grown on an 8-well chamber slide to 60-70% confluency. The cells were rinsed twice with PBS and fixed with 4% paraformaldehyde for 10mins at room temperature. The cells were then washed twice in PBS and permeabilized with 0.5% NP-40. After washing again, the cells were blocked with a mixture of Cold Water Fish Gelatin with BSA dissolved in PBS (PBG) for 1 hour followed by overnight incubation at 4ºC with primary mouse monoclonal antibody (anti-folate, at 2.5µg/ml; Enzo Life Sciences) diluted in PBG. The cells were then washed with PBG 3 times and treated with secondary antibody (goat anti-mouse IgG conjugated to Alexa 488 at 1µg/ml dilution; A11029 Invitrogen) also diluted in PBG. The cells were next washed 3 times in PBG and then covered with embedding media mixed with DAPI (Sigma-Aldrich, St. Louis, MO) and Vectashield mounting media (Vector Laboratories, Burlingame, CA). We used 200µg/ml of DAPI in a 1:1000 volume dilution with mounting media.

Survival/Cytotoxicity Assay: To assay potential toxic effects of dye-loaded TCRNs, $1x10^4$ M12 or SCP cancer cells were seeded (~50-70% confluency) in 6-well chambers filled with 1ml of their respective media. The cells were allowed to acclimate and attach to the plates for 2-4 days. The cells were treated with TCRNs at varying concentrations for 6-168 hours. At each time point (6, 24, 48, 72 and 168 hrs), cells were collected after treatment with 0.25% (w/v) trypsin-0.1% (w/v) EDTA (Mediatech, Inc .,Manassas, VA), centrifuged, and resuspended in 2mls of

respective culture media. Live/dead counts were performed using a hemocytometer after Trypan Blue treatment (4% w/v) in normal saline (Mediatech Inc) at a dilution of 0.5mls cell suspension with an equal volume of 50% Trypan blue. Cell survival was evaluated at defined time intervals of exposure by live cell counts expressed as a percentage of total cells counted. Using Nile Red (NR) and Dimethyl Indole Red (DiR), cells were treated to the following dilution scheme: NR (PBS, 3.4µg/ml, 0.68µg/ml, 0.34µg/ml. 0.034µg/ml, and 0.0034µg/ml), DiR (PBS, 40µg/ml, 8µg/ml, 4µg/ml, 0.4µg/ml, and 0.04µg/ml). It should be noted here that when calculating TCRN doses and concentrations, one must consider both the concentration of the NP and the concentration of the dye contained in the NP. For the sake of simplicity, all concentrations given refer to the concentration of the dye contained within the NP since this would, by inference, represent the concentration of drug administered to the animals would.

Confocal Microscopy: In 6-well chambers filled with 1 ml of respective media, $1x10^4$ SCP cells or M12 cells suspended in 0.1mls of media were seeded (50-70% confluency) onto $22mm^2$ acid cleaned and flame dried cover slips. The cells were allowed to acclimate and attach to the slides for 2-4 days. We delivered a standard 0.1 ml volume of the various NP dilutions into 2.8ml of RPMI culture media in each well. The cells were treated with the dye loaded TCRNs at various dye concentrations at time points ranging from 6-168 hours. At each time point, cells were fixed with 4% paraformaldehyde in PBS for 10mins, washed with 0.3M glycine in PBS (3x) for 10mins, and mounted on a slide with DAPI (Sigma-Aldrich, St. Louis, MO) and Vectashield mounting media (Vector Laboratories, Burlingame, CA) using 200µg/ml DAPI in a 1:1000 dilution with mounting media. Slides were stored in a light proof box at 4ºC until imaged. Cell imaging was performed using either a Zeiss LSM 510 META confocal microscope or the Leica

TCS-SP2 AOBS confocal microscope. Images were acquired and processed with imaging software provided by the respective microscopes. For our confocal imaging, we originally chose DiR as our fluorescent dye because it is lipophilic and easily intercalates with cell membrane structures. It has a higher emission spectra enabling better tissue penetration during Xenogen imaging. DiR emits in a range that is near infrared fluorescence (excitation 750nm/emission 780nm). It is also a lipophilic carbocyanine that is weakly fluorescent in water but highly fluorescent and quite photostable when incorporated into membranes. It has an extremely high extinction coefficient and short excited-state lifetimes (~1 nanosecond) in lipid environments (35). Once applied to cells, the dye diffuses laterally within the plasma membrane (36). This dye was recommended and was ideal for the *in vivo* component of our experiments, but, with the confocal microscopes that are commonly used for our *in vitro* experiments, the spectra of excitation of this dye is too high for the lasers used. Furthermore, using the laser that is most suited for this dye could also impact cell architecture and distort our images. To address this problem, we switched to using Nile Red (excitation 559/emission 636) for the preliminary *in vitro* experiments. NR is a phenoxazone dye that fluoresces intensely in organic solvents and hydrophobic lipids. The fluorescence, however, is fully quenched in water and therefore acts as a fluorescent hydrophobic probe (37).

***In vivo* imaging:** The tumor mouse model was generated by SC injection of 5×10^6 M12 or SCP cells in PBS into the dorsolumbar region of male and female athymic nude mice (5–6 weeks old). The mice were subject to imaging studies when the tumor volume reached a size around 1.0 cm^3. All animal experiments were performed in compliance with VCU's Institutional Animal Care and Use Committee (IACUC). This *in vivo* experiment used subcutaneous M12 and SCP

xenograft tumors in athymic nude mice. Once tumor sizes reached an initial diameter of about 0.5-1.0cm, the mice were treated intravenously with TCRNs loaded with dye at 2 different concentrations. Briefly, using a total of 5 mice per treatment group, animals were injected intravenously once in the tail vein or the retro-orbital plexus with approximately 100µl of the dye loaded TCRN mixture at various concentrations. At predetermined time points (from 0 to 168 h post-injection), these mice were anesthetized with a ~3% isoflurane/oxygen mixture and placed in the dark chamber of the IVIS Imaging System 200 Series® *in vivo* Xenogen® imaging instrument. The image was created using the ICG Bkg/ICG and the GFP Bkg/GFP excitation and emission filters. The quantitative distribution of TCRNs in the animal was determined by fluorescence measurements using vendor software. The total fluorescence efficiency for the tumors was measured using a uniform region of interest (ROI) applied to each tumor with background from the control value. Image analysis was made using Living Image® software v2.60.1.

Chapter 3

Results

Hypothesis: We propose that TCRNs carrying fluorescent dyes will selectively deposit their contents into the cytoplasm and the nucleus of carcinoma cells via the FA/FR interaction, producing changes in fluorescent signaling as measured and visualized by *in vitro* and *in vivo* assays.

Specific Aim 1: To characterize and verify the FR profile of our prostate and breast cancer cell lines in order to make meaningful correlations regarding the TCRN's ability to target our cells using this receptor.

Rationale: Our TCRNs are tagged with a FA moiety in order to exploit the fact that several malignant tumors are known to over express the FR. Once we confirm the FR profiles of our cells, we can then use the FR/FA interaction to selectively target cells using the TCRNs allowing us to attach even greater clinical relevance to our NPs.

In vitro assays verify differential FR expression on breast and prostate cancer cells

There are many factors influencing the successful delivery of TCRN agents to the cells. Our experiments focused on one of those factors, the expression of FRs on the cell surface of the prostate and breast cancer cells. TCRNs are designed to use the FR to target cells for delivery of their contents. Using multiple protein-based assays, we verified and quantified the presence of

the FR on the cells selected for this study. Western results confirm that the FR protein is expressed by breast and prostate cancer cells, but to varying degrees. As expected, our results showed that the breast cancer cell lines (SCP and MDA-231) express the FR at higher levels than the prostate cell lines (M12 and M12-luc) (Figure 5) (12, 24). It is also worth noting that our Western showed that the BJ fibroblasts also strongly expressed the FR. Based on reports in the literature, we would not expect that this protein would be expressed primarily on the cell surface, although this finding may suggest the expression of the FR in the cytosol since whole cell lysates were used. To confirm this, we would need to subject the BJ fibroblast cells to the FACS assay and a radioligand binding assay for comparison with our breast cancer prostate cancer cells.

The results of the Western were further confirmed with a FACS analysis showing the prevalence of the FR on the cell surface of intact cells. Flow cytometry is broadly defined as a system for measuring and then analyzing the signals that result as particles flow in a liquid stream through a beam of light (38). Treated cells are collected and suspended in PBS, and the cells are then injected into the flow cytometer. When coupled with fluorescent probes, it enables Fluorescence-Activated Cell Sorting (FACS) analysis, which is an ideal tool for sorting heterogeneous mixtures of cells based on their cell surface profile. This technology can sort cells according to their fluorescent intensity and size. In this FACS analysis, the cells were probed with primary antibody against the FR and a secondary antibody flagged with the Alexa 488 fluorophore. Our FACS analysis for the FR (Figures 6-10, summarized in Table 1) showed that the breast cancer cell line (MDA-MB-231) had increased levels of FR when compared with the prostate cell lines tested (M12 and M12-luc). Based on this data we would expect that our FA-labeled TCRNs would be able to interact with these FR-expressing cells in a way that would permit them to transport their contents into the cells. Further, we would expect that cells with a

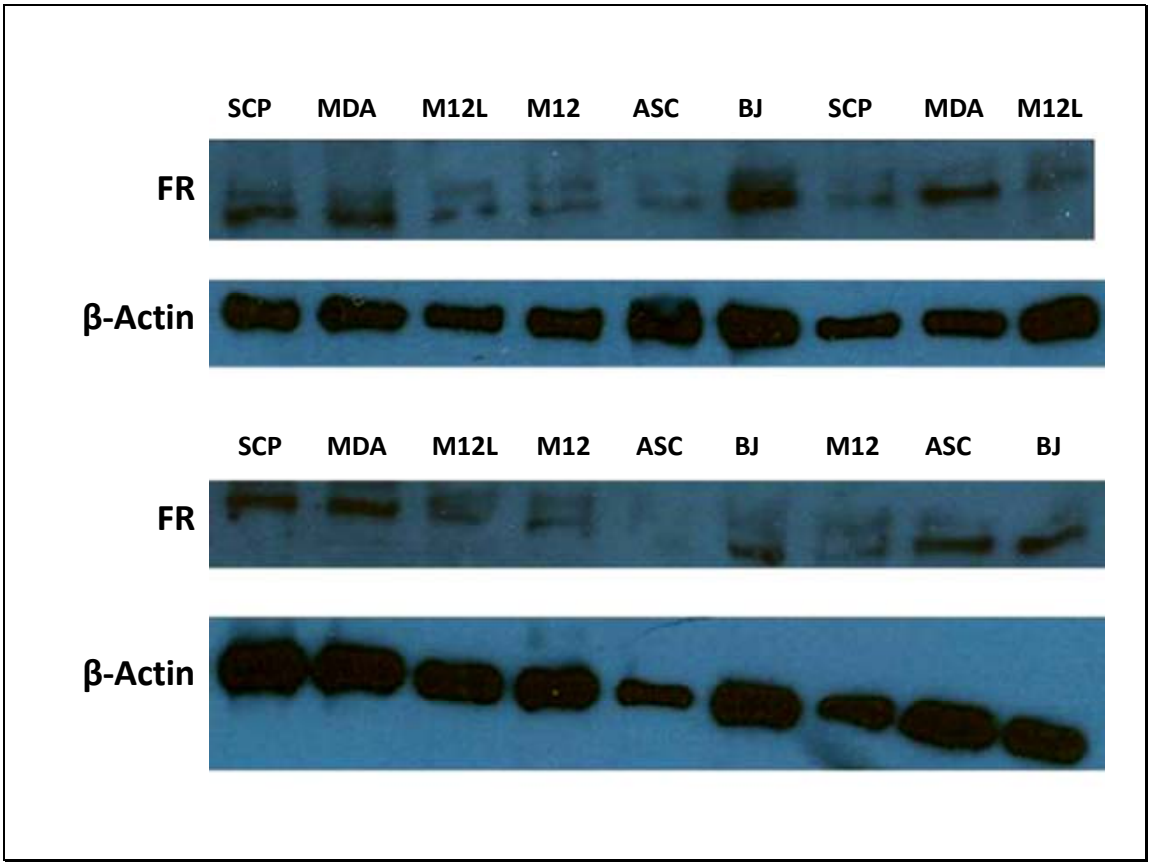

Figure 5: Western Blot Assay Probing for the Folate Receptor (FR). The Western blot shows confirmation of the literature's claim that prostate cancer cell lines (M12L and M12) express the FR to a lower degree than the breast cancer cells lines (MDA and SCP). BJ fibroblast and ASC cells were included as normal cell comparisons, with minimal expression in ASCs and higher expression in BJ. Multiple independent protein isolations from each cell type are shown. The loading control used is β-actin.

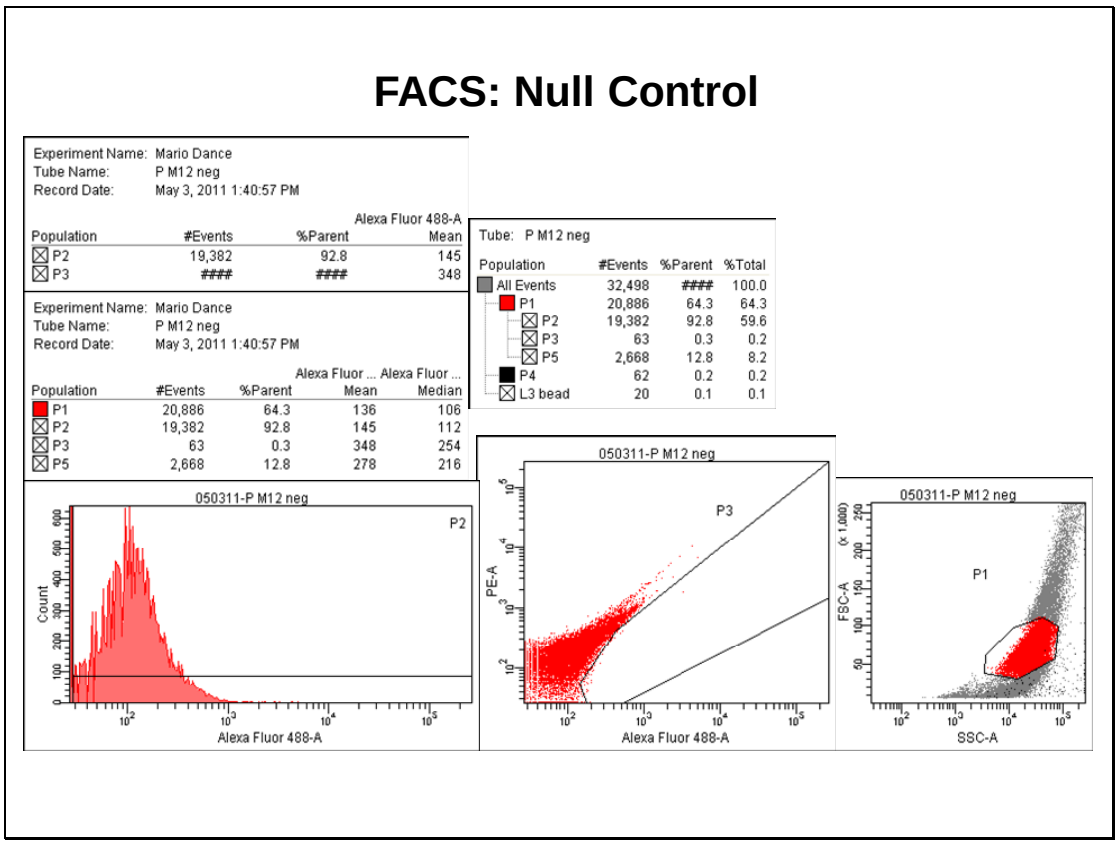

Figure 6: FACS Analysis Showing Poor Alexa Fluor-488 Signal in Null Control. These data sets show that M12 prostate cancer cells not probed with any primary or secondary antibodies have a very low fluorescent intensity and, therefore, were used to determine background signal (i.e., autofluorescence) generated. Similar results were obtained with the MDA-MB-231 cell types.

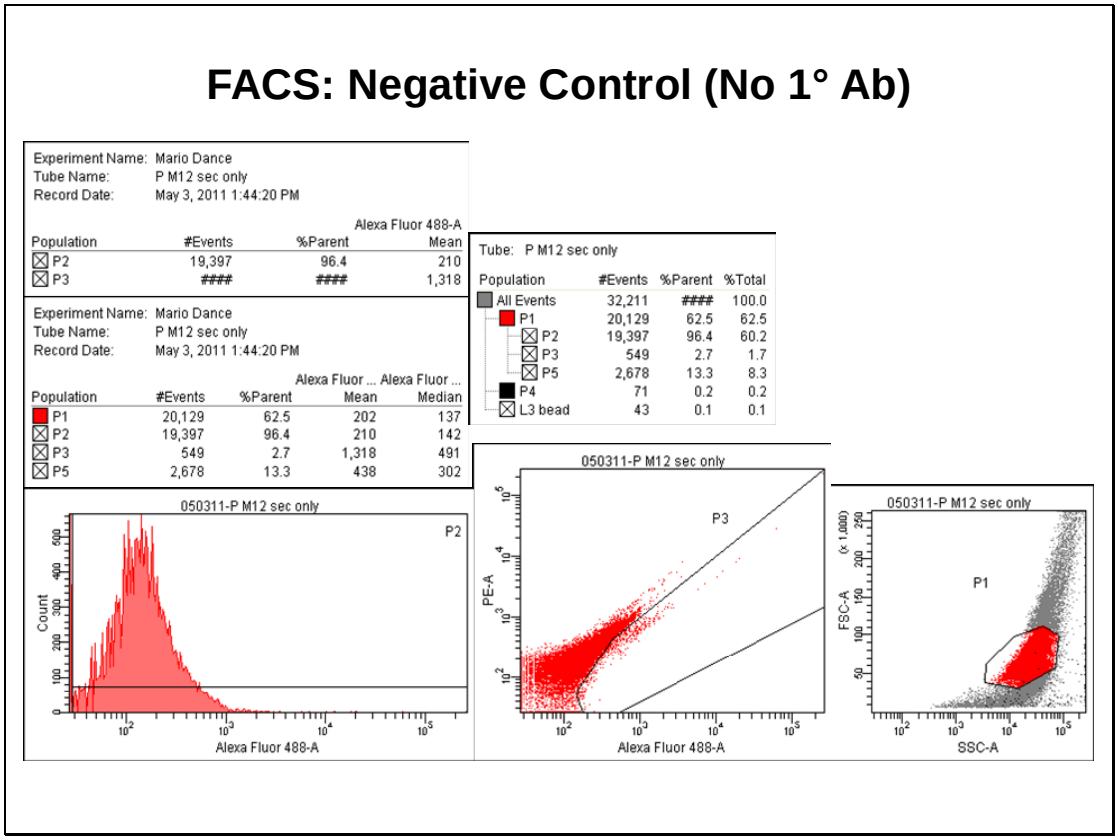

Figure 7: FACS Analysis Showing Poor Alexa Fluor-488 Signal in Negative Control. This data set shows M12 prostate cancer cells that were not incubated with a primary antibody but were probed with the secondary antibody alone. These results were used to determine background signal generated by cells as a consequence of exposure to secondary antibody only, as well as any fluorescence associated with experimental manipulation. Similar results were obtained with the MDA-MB-231 cell types.

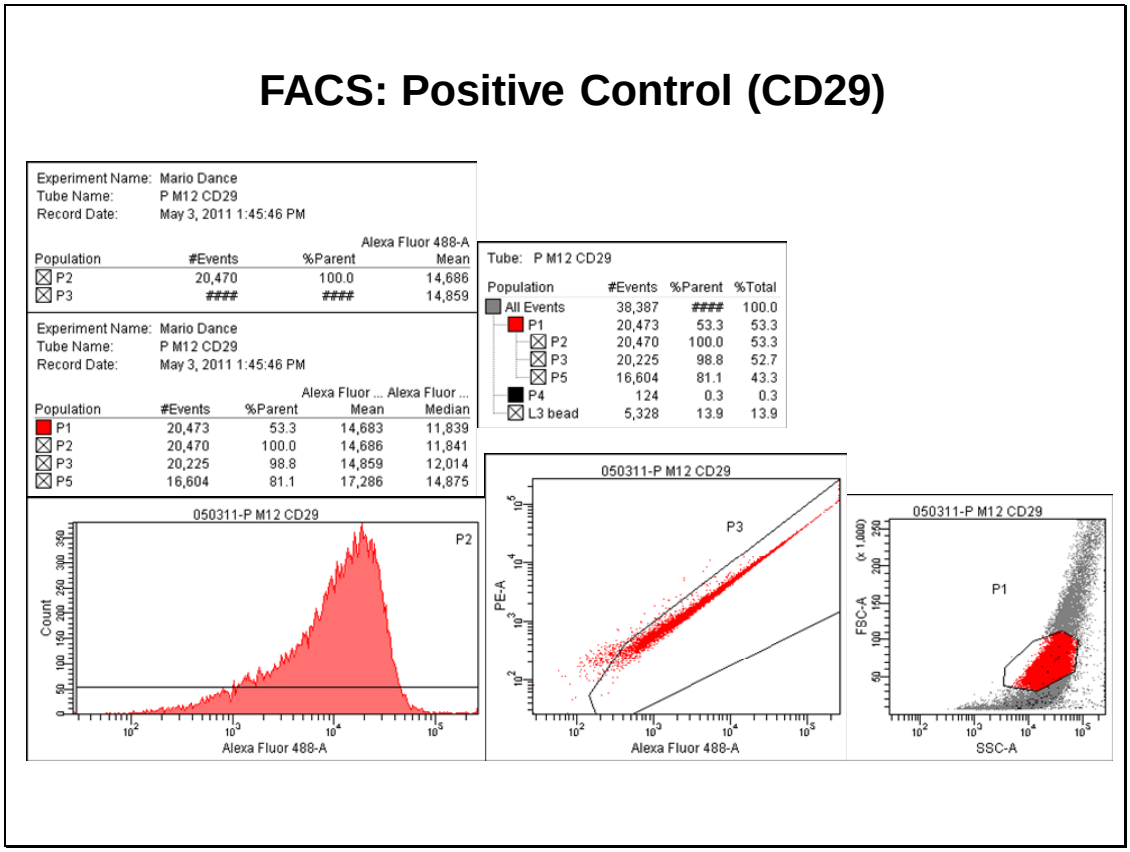

Figure 8: FACS Analysis Showing Strong Alexa Fluor-488 Signal in Positive Control. This data set shows M12 prostate cancer cells that were probed with anti-CD29 primary antibody and the secondary antibody. This sample shows that our FACS assay is optimized and able to detect a ubiquitously expressed cell surface antigen when probed. Similar results were obtained with the MDA-MB-231 cell types.

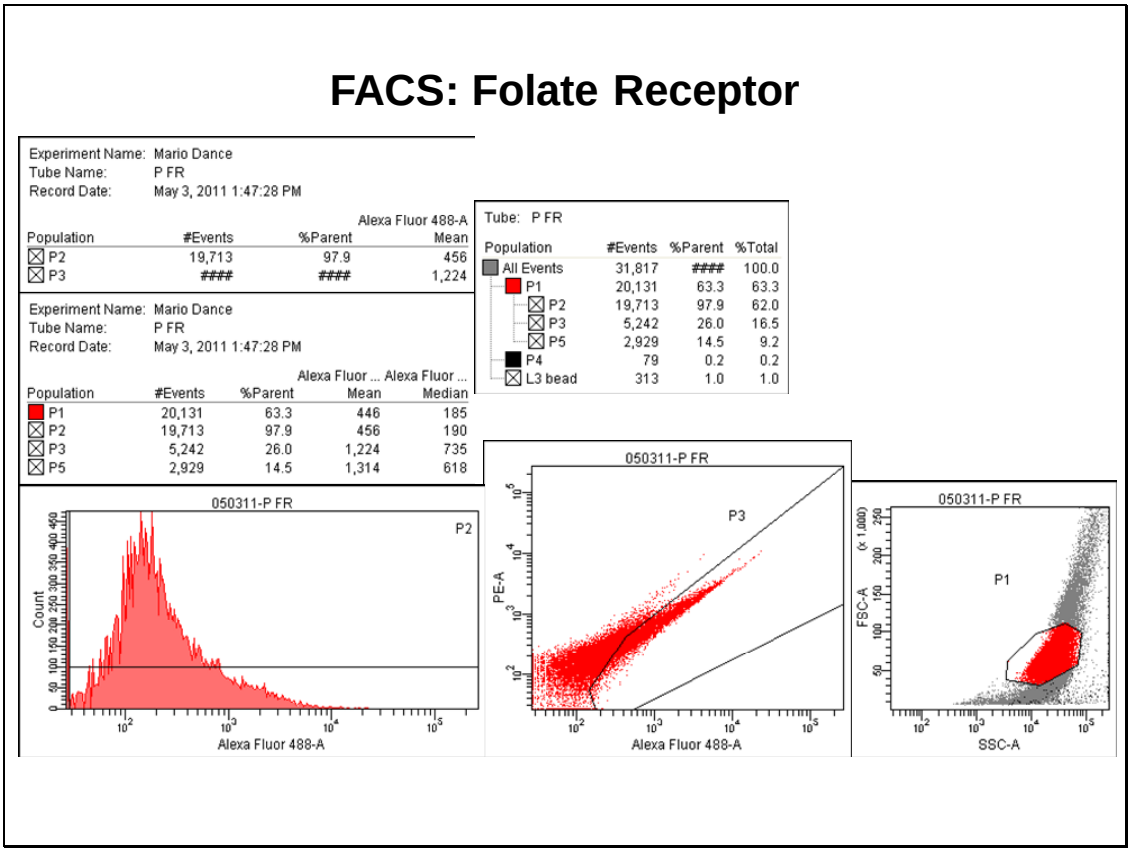

Figure 9: FACS Analysis Showing Weak-Moderate Alexa Fluor-488 Signal in a Probe for the FR (M12). This data set shows M12 cells that were probed with the aim of detecting cell surface FR. Cells were probed with anti-FR primary antibody and the secondary antibody. This experiment shows us the strength of the FR protein expression on the cell surface.

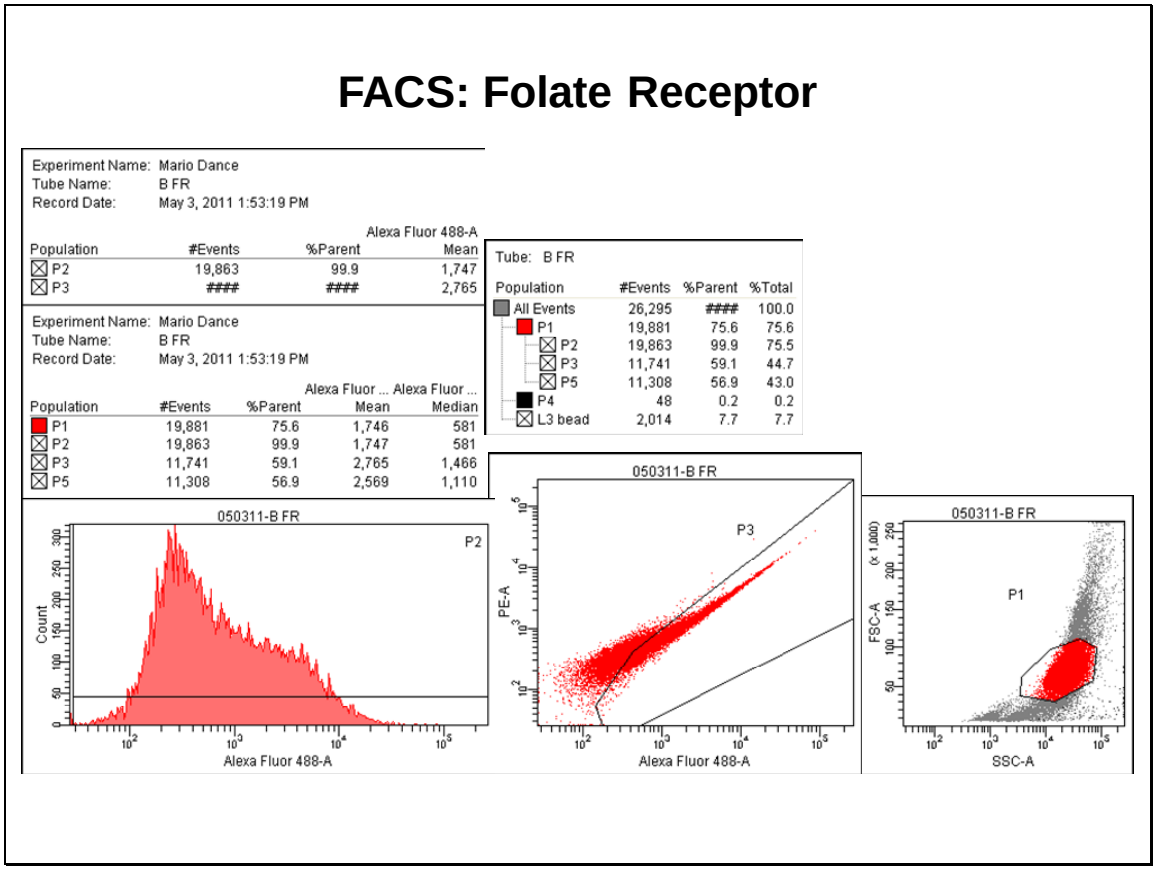

Figure 10: FACS Analysis Showing High Alexa Fluor-488 Signal in a Probe for the FR (MDA-MB-231). This data set shows MDA-MB-231 cells that were probed with the aim of detecting cell surface FR. Cells were probed with anti-FR primary antibody and the secondary antibody. This experiment shows us the strength of the FR protein expression on the cell surface.

Table 1. Summary of FACS Data

Cell Line	Antibody Probed	P1 % Gated segment	P2 Ave Alexa Signal	P3 % positive
M12	O	64	145	0.3
M12	2° only	62	210	2.7
M12	CD29	53	14,686	98.8
M12	FR	63	456	26
M12	PSMA	58	3,404	44
M12 Luc	O	56	275	0.3
M12 Luc	2° only	52	278	6.6
M12 Luc	CD29	50	12,928	99.3
M12 Luc	FR	52	555	30.7
M12 Luc	PSMA	53	2112	53.3
MDA	O	75	180	0
MDA	2° only	79	229	1.1
MDA	CD29	76	21,575	99.2
MDA	FR	75	1,747	59.1
MDA	PSMA	76	730	36

Table 1: Summary of Data from FACS Experiments. P1 indicates the percentage of the total parent population of cells that were assayed for the receptor in question. P2 indicates the average strength of the Alexa 488 signal generated by the cells that were assayed from this subpopulation. P3 indicates the percentage of cells that produce a signal that are positive for the receptor being probed after accounting for background signal. These results confirm what we see in the western and IHC assay characterization of FR. MDAs express FR to a higher degree than the M12's.

stronger FR profile would have a measurably and significantly greater ability to internalize the TCRNs than cells with a weaker FR profile. The difference in FR expression was confirmed definitively using live cell FACS analysis and less definitively using IF Microscopy (Figure 11). Together our data suggests that the FA/FR system will be useful for our TCRNs to deposit their fluorescent dyes in FR-expressing carcinoma cells when compared with those cells that express lower levels of FRs.

In our FACs assay, we also probed for the prostate specific membrane antigen (PSMA) (see Table 1). Recent studies have shown that this membrane bound protein can also be used by cells to transport FA into cells (39). The presence of this protein in our cells could potentially influence the uptake of our FA conjugated TCRNs, especially with respect to our prostate cancer cells that show a reduced level of FR compared to the breast cancer lines. While we did not perform any experiments that would specifically target this protein using the TCRNs, it is important to factor its expression into any results that make use of the FA/FR interaction as PSMA can also internalize FA. The presence of this protein in our M12 cells cells could potentially lend greater weight to the importance of the FA moiety on our TCRNs and provide an alternative method for exploiting this interaction in other cells, especially prostate cancer cells.

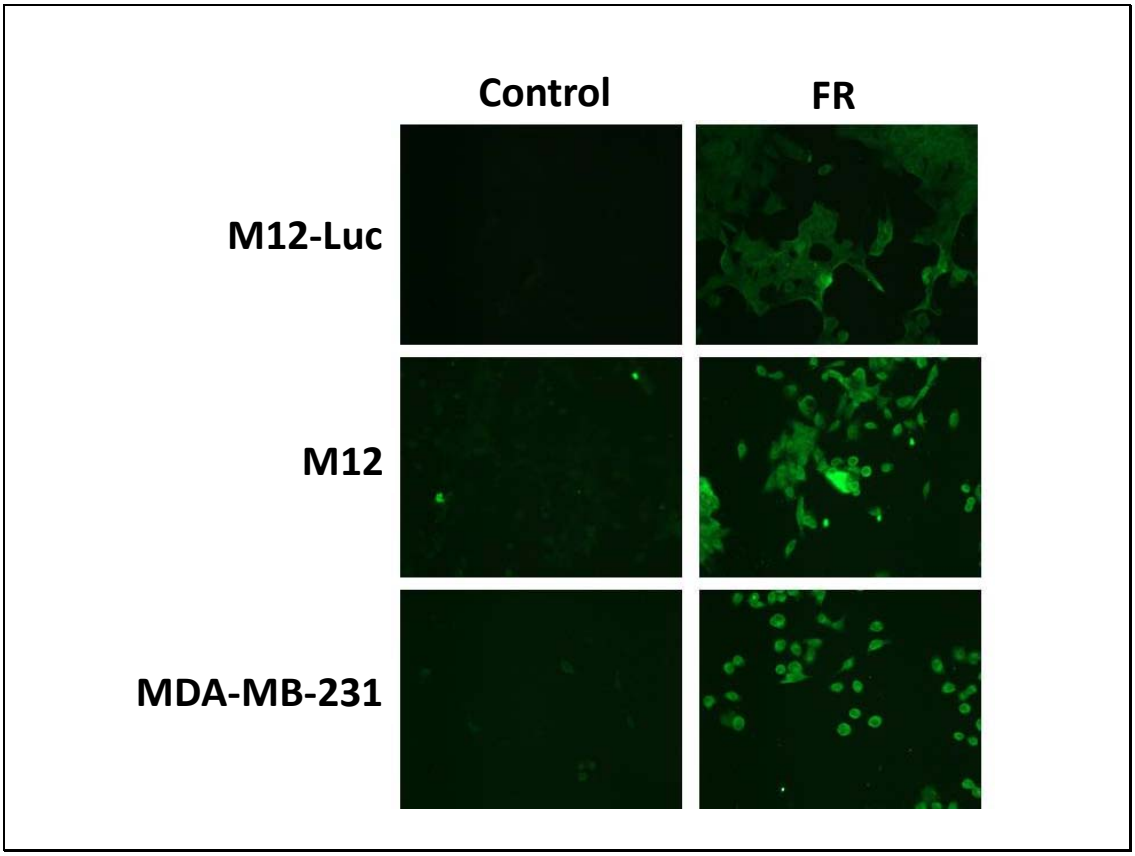

Figure 11: Immunocytochemistry Assay Showing Folate Receptor expression in M12 prostate and MDA-MB-231 breast cancer cells. Shown, imaged at 60x magnification, is a stronger fluorescent signal produced by cells when probed for the FR. FR protein is detected in the 3 cell lines but seems to be slightly stronger in MDA-231 cells. Control cells were probed with 2° antibody alone.

Specific Aim 2: To demonstrate TCRN dye delivery to cells correlating TCRN function with the FR using differences in fluorescent signaling within the cytoplasm and the nucleus of our cells

Rationale: Because there are studies that suggest that the TCRNs can carry and deposit their contents into the nucleus of cells grown *in vitro*, we believe that if this data can be verified in additional cell lines using different agents *in vitro* and then *in vivo* we can then infer that the TCRNs have the potential to be used to carry chemotherapeutic agents in a clinical setting.

***In vitro* cytotoxicity suggests optimal TCRN dose**

In general, any novel NP is considered to be a potential biological hazard, making it critical to evaluate any potential *in vitro* cytotoxicity related to the TCRNs that could interfere with our study. Once safety can be demonstrated using TCRNs carrying biologically inert dyes, then we can infer that the TCRNs may be used to carry other more biologically active agents that may have their own cytotoxic effects, which will also enable us to restrict our interpretations regarding efficacy to the agent and not to the carrier. Using a dose response curve, we were able to determine an optimal concentration of the TCRNs that enabled normal cell proliferation, which suggests a starting point for an *in vivo* dosage for assessing toxicity in mice.

This experiment provided optimal conditions for cell growth in the presence of the dye-loaded TCRNs. The experiment shows that the optimal dilution of dye for cell survival of both cell types was the 1:100 dilution of the nanoparticles, which corresponds to the 0.4µg/ml treatment for DiR and the 0.034µg/ml treatment for NR (Figures 12, 13). Cell survival was also highest at 24 and 48 hrs post inoculation. Our data demonstrate that TCRNs loaded with dye do

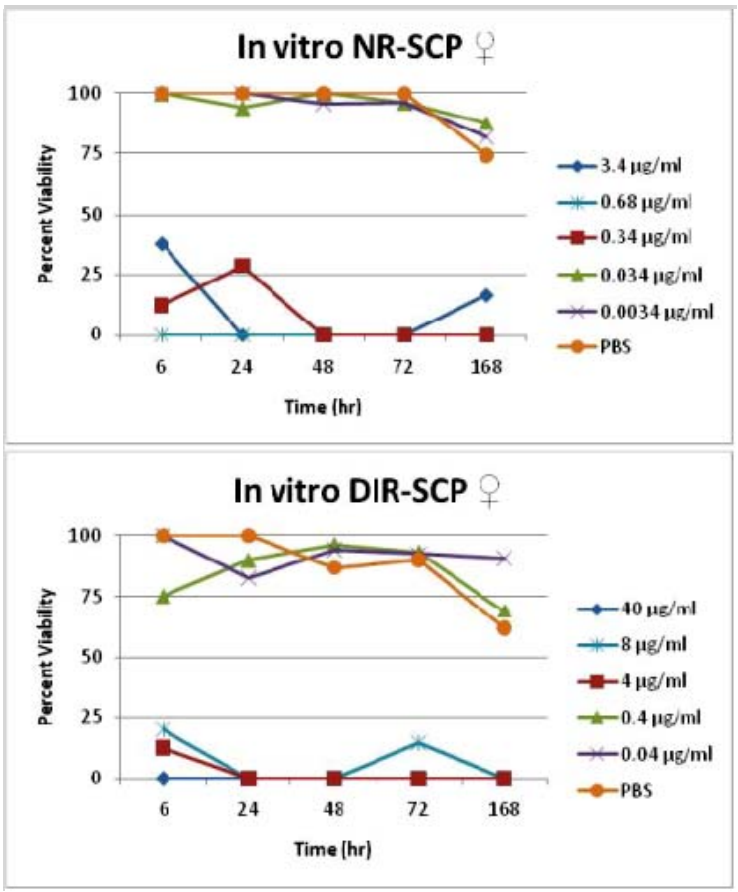

Figure 12: Percent viability of SCP breast cancer cells treated with dye loaded TCRNs over time. These graphs show that the highest dosage of the dye loaded TCRNs that can support cell growth over time without adverse affects is 0.034µg/ml (Nile Red) and 0.4µg/ml (DiR). This suggests a dose dependent toxic affect associated with the TCRNs in this cell line.

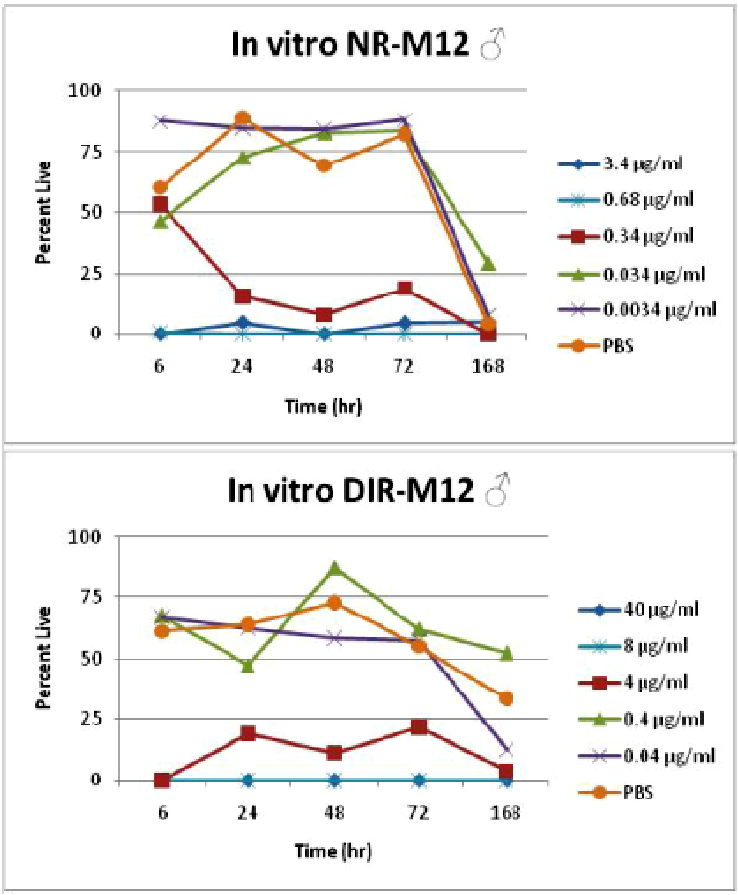

Figure 13: Percent viability of M12 prostate cancer cells treated with dye loaded TCRNs over time. These graphs show that the highest dosage of the dye loaded TCRNs that can support cell growth over time without adverse affects is 0.034µg/ml (Nile Red) and 0.4µg/ml (DiR). This suggests a dose dependent toxic affect associated with the TCRNs in these cells.

impact the survival of both the SCP and the M12 cell lines and that there is a toxic effect related to the TCRNs especially at the higher concentrations of dye. The results indicate that the highest concentration of DiR for both cell types is 0.4µg/ml and 0.034µg/ml for NR. These values correspond to NP concentrations of 30µg/ml and 0.3µg/ml respectively.

Confocal Microscopy shows nuclear association of TCRN dye.

The confocal assay of this experiment was complicated by many technical challenges. The TCRNs have a very short shelf life (approximately 3 weeks) and so many of the *in vitro* and *in vivo* experiments had to be performed at the same time once the TCRNs were made. There were also technical issues associated with the confocal microscopy, which was discovered after processing the images. The use of the Leica microscope provided little, if any, capability to distinguish subcellular localization (Figure 14, lower panels), while the Zeiss confocal microscope showed definitive localization of the dye-loaded TCRNs Figure 14, upper panels). Further examination of the confocal images suggested that, at a minimum, the TCRNs can enter cells and deposit their contents into the cytoplasm. It appears that they travel and associate with the nucleus and possibly deposit a fraction of their contents into the nucleus (Figure 14). The peak effect noted in this experiment parallels the survival experiment and shows that the strongest fluorescent signal for the NR dye occurs in the 1:100 dilution between 24-72 hours post incubation with the TCRNs.

***In vivo* parenterally administered TCRNs fail to show tissue specificity.**

Extrapolating *in vivo* dosing from our *in vitro* experiments was a challenge, but, in this experiment, it was useful to correlate the concentration of the TCRNs with the dye within the

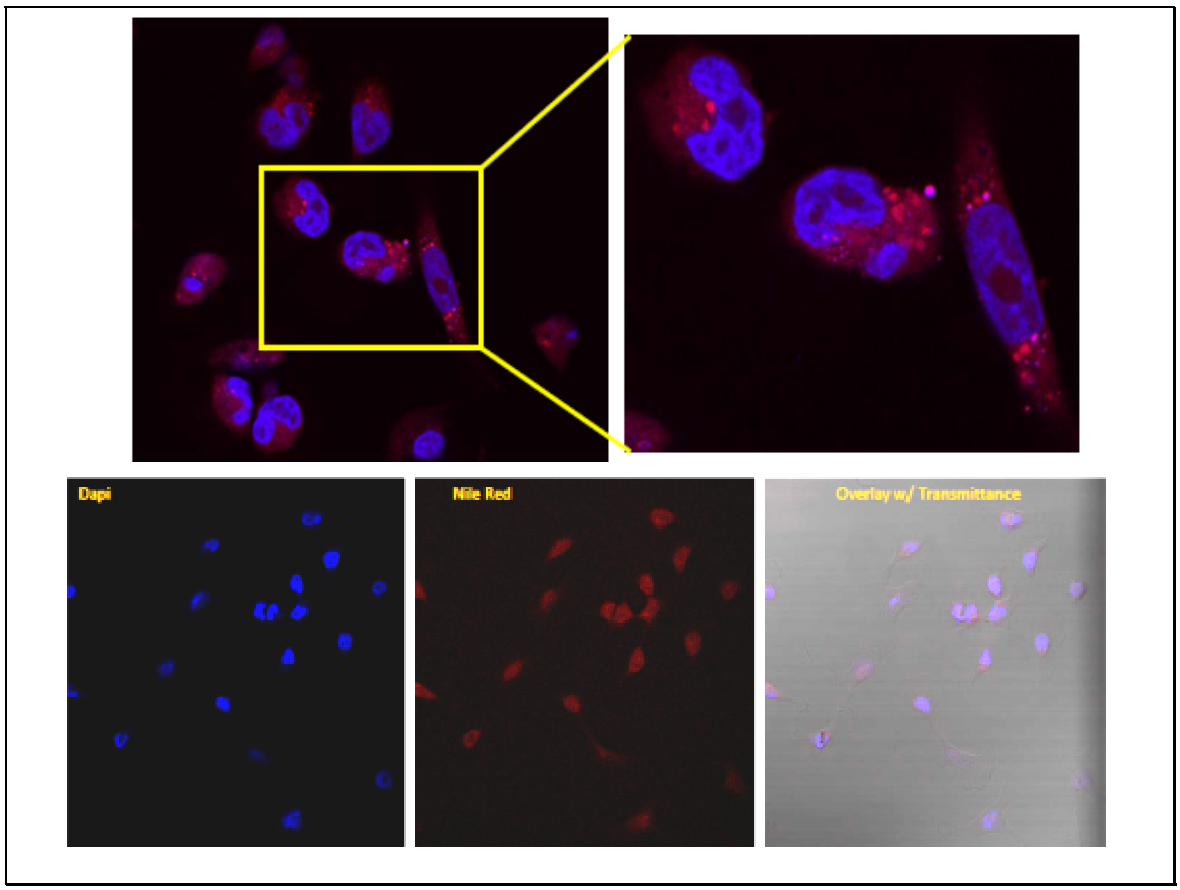

Figure 14: Zeiss and Leica confocal images of SCP28 cells grown *in vitro* at 1:100 dilution of NR loaded TCRNs and 48hrs post treatment. Representative images of the same cells taken with 2 different microscope systems showing the qualitative differences noted between the two systems. The top images were obtained using the Zeis microscope. Nuclei are stained with DAPI and nucleus is dotted with red staining likely resulting from deposition of NiR dye. Magnified image is shown to the right, with punctuate TCRNs localizing in the perinuclear region of the cell. The bottom images were obtained using the Leica microscope. The image shows that the nuclei are stained with DAPI and that those nuclei staining red may be the result of deposition of NiR dye, although this is unclear. This data suggests that there were notable differences in cells viewed under Leica vs. Zeis confocal microscopes and that TCRNs are localized near the nucleus but there is no clear evidence of nuclear delivery.

blood stream with the concentrations of TCRNs that are used in the media in our *in vitro* cytotoxicity experiments. Blood volume in animals is estimated using the following formula: body weight (kg) x 7% = total blood volume (L) (40). For a typical mouse of about 20-40g, we can calculate a total blood volume of 2.5mls. In our initial *in vivo* experiments, we delivered the dye-loaded TCRN in a 0.1ml total volume. We also noted that the highest concentration of the dye/TCRN solution that could be given to the animals without noticeable and consistent toxic effects was 36µg/ml of DIR dye and 30mg/ml TCRN NPs. In a 20g mouse (blood vol ~1.5mls), this translates to a dose of roughly 180µg/kg of dye or a blood concentration of dye equal to 2.4µg/ml. The lowest treatment administered in this experiment corresponds to a dosage of 60µg/kg of dye or a blood concentration of dye equal to 0.8µg/ml, which parallels studies of these classes of drugs suggest as being well within a tolerable range.

Based on our *in vitro* data and the literature, we predicted that TCRNs carrying fluorescent dyes would selectively target tumor cells, differentially depositing their contents into the nucleus of carcinoma cells in a way that produces changes in fluorescent signaling. Here we are only able to determine if dye is selectively deposited into the tumor tissue, and we infer from our confocal studies that if the dye can be selectively focused in the tumor tissue, then it will deliver its contents to the cells in the same manner noted in confocal microscopy. We measured the fluorescent signal in the tumor using *in vivo* bioluminescent/fluorescent imaging with XIT at various time points for one week. We found that the TCRNs are clearly being deposited in the animals and that the particles persist in tissue without significant selectivity for the tumor tissue (shown in Figures 15 and 16, and quantified in Figure 17).

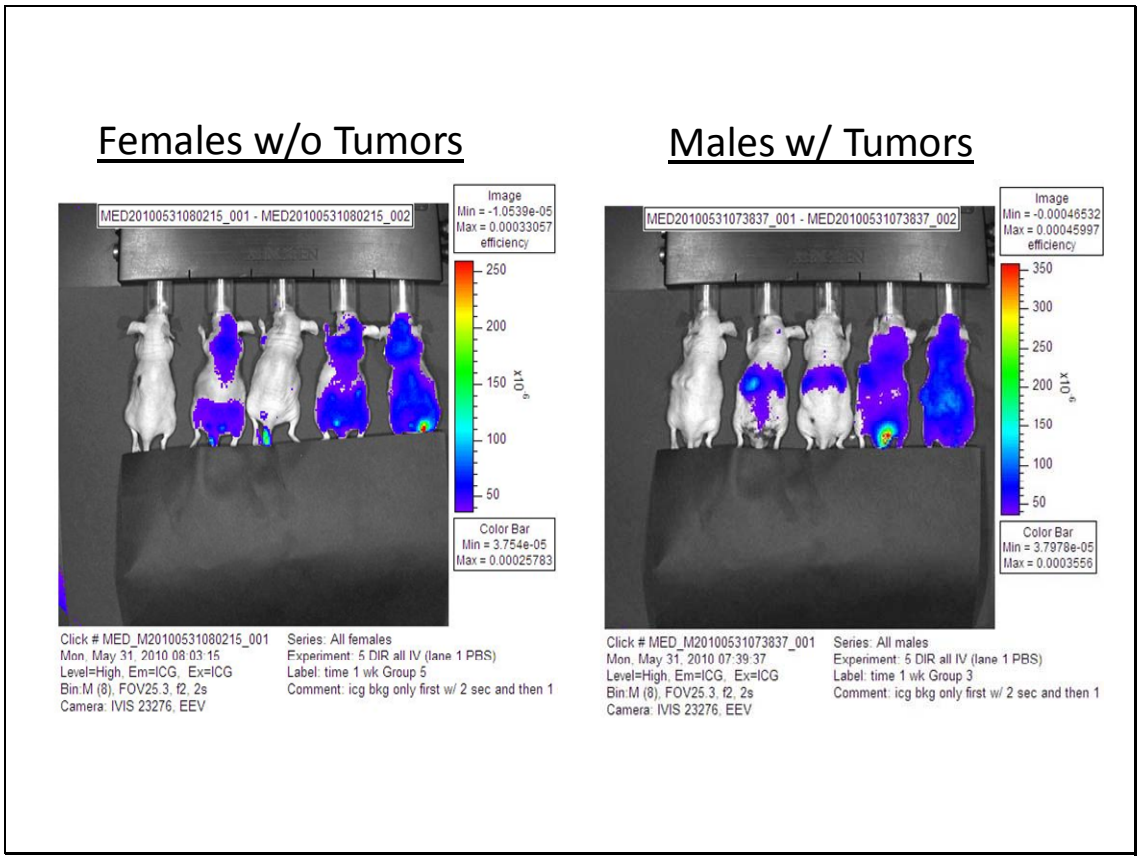

Figure 15: Representative imaging of TCRN fluorescent signal (DiR) using Xenogen Technology. These images represent fluorescent signal from the nanoparticles after 1 week of incubation in athymic nude mice, either without tumor (Females w/o Tumors) or after injection with M12 prostate cancer cells (Males w/ Tumors).

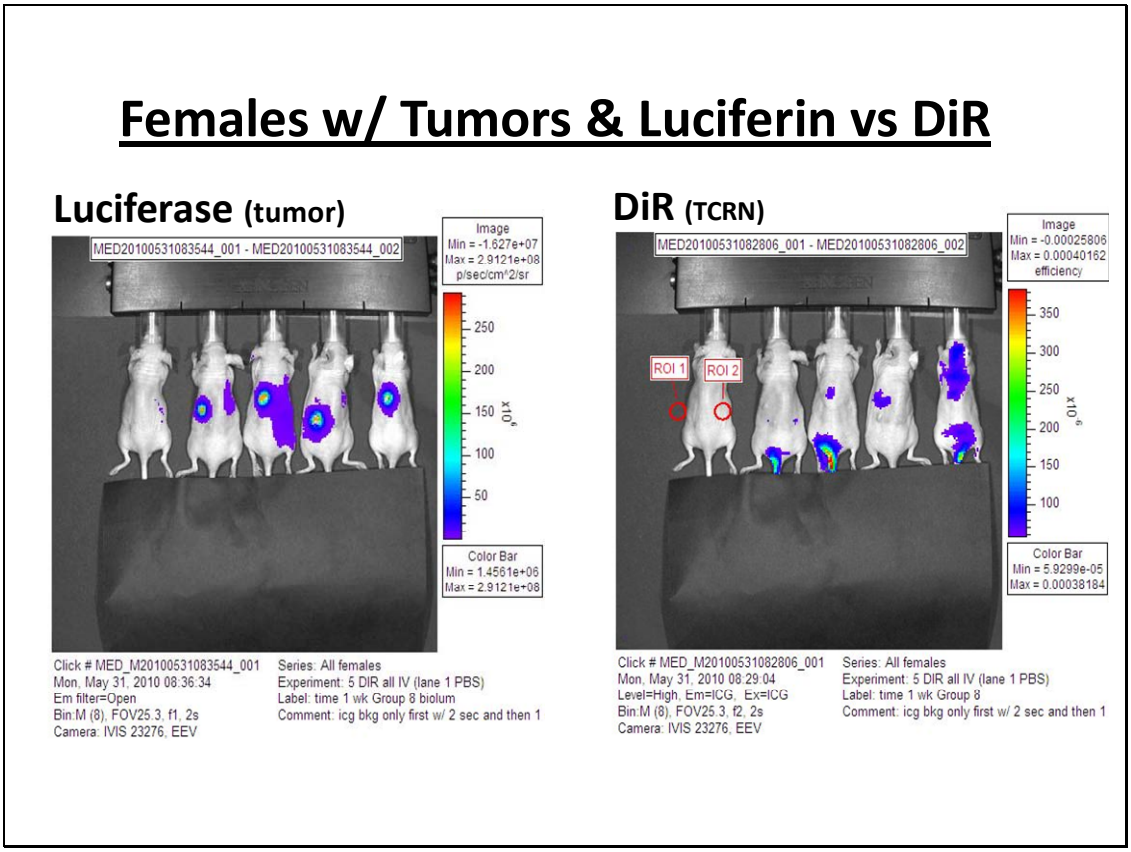

Figure 16: Representative Xenogen images of female mice with tumors measured at 7 days. The fluorescent signal of xenograft tumors measured in female is shown for D-luciferase (tumor fluorescence) and DiR (TCRN fluorescence), showing minimal overlap of nanoparticle and tumor.

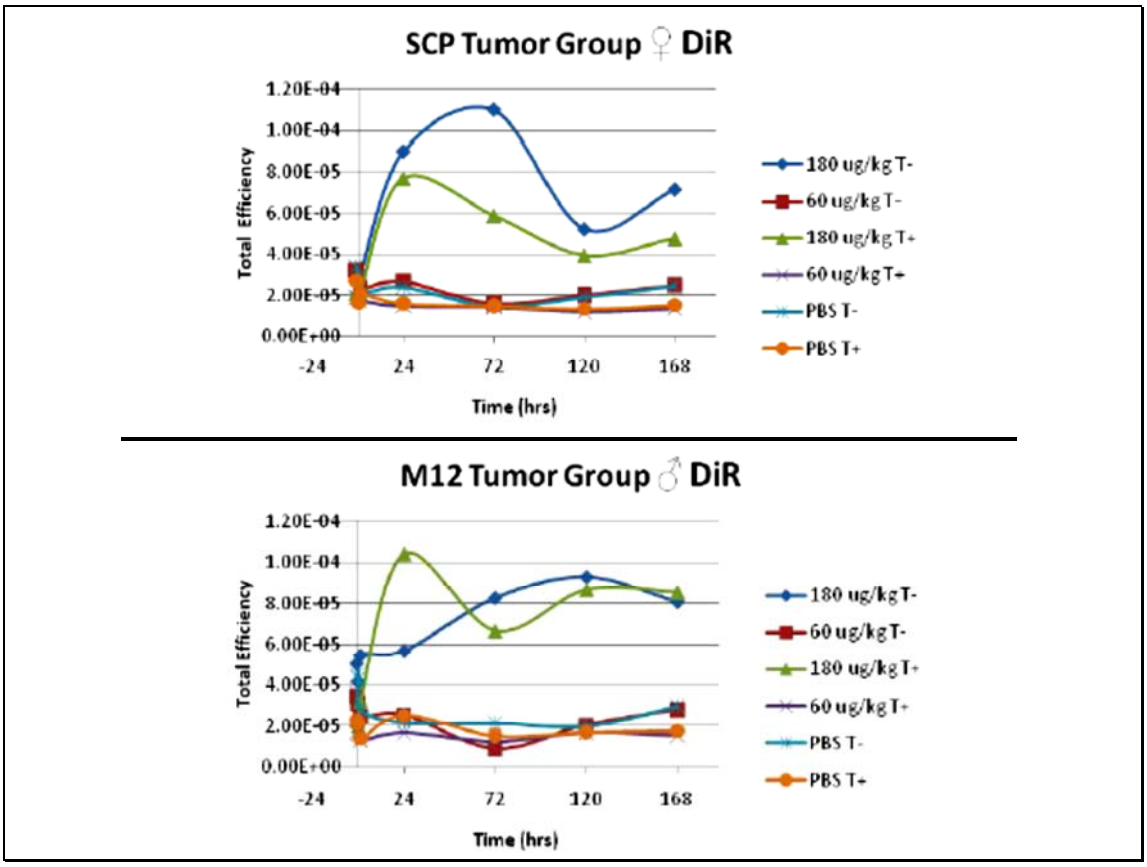

Figure 17: Fluorescent signal measured over time using Xenogen Imaging Technology. These graphs show the fluorescent signal of xenograft tumors measured in female (top) and male (bottom) mice and recorded over time for 6 groups. The groups represent the various doses of DiR dye delivered by the TCRNs. Mice with tumors (T+) are compared with mice lacking tumors (T-). This data suggests that tissue deposition occurs without apparent selection of tumor tissue.

The *in vivo* Xenogen studies were subjected to complex statistical analysis using sophisticated regression analysis with multiple variables and it was determined that the differences noted between the treated and non treated animals was not significant. The strength of our *in vitro* conclusions derives from the fact that we confirmed the results in one assay using complementary assays. Statistical analysis for most of our *in vitro* experiments was moderately limited because of the lack replicate experiments for the confocal and FACS analyses and because Western densitometry is historically not quantitative. Importantly, the Western assays were repeated, showing remarkable similarity in the overall expression levels for each cell type, including breast and prostate cancer and the 2 normal cell types, BJ fibroblasts and ASCs. In general, our results clearly show that the FR is expressed at higher levels in breast tumor cells and to some degree in prostate tumor cells using 3 different techniques. The *in vivo* results, while not statistically significant in terms of TCRN-tumor co-localization, were important and definitive in showing localization of the TCRN in the animal and retention of the nanoparticle for more than 5 days without liver toxicity and/or excretion by the mice. Taken together, our results suggest that TCRNs have the ability to target the FR in tumor cells and be effectively delivered at or near the nucleus of the cells, while showing stability after delivery into tumor bearing animals.

Chapter 4

Discussion

Even the briefest review of the current literature related to nantotechnology will convince one that this field is explosive, one that is ripe with potential for advances especially in the area of biomedical applications. Because the field is so young, much work needs to be done using *in vivo* systems. Although ambitious, our proposal tried to confirm the *in vitro* experiments associated with the TCRNs with *in vivo* experiments. There is much that can be said about these NPs after our experiments, but there is still much more that needs to be done before definitive conclusions can be made about them.

Our TCRN was tagged with a FA moiety in order to exploit the fact that many cancers over-express FRs while most normal tissues express low to negligible levels. This FA/FR interaction would help to show the clinical significance of the TCRNs. Furthermore, the literature confirms that the over-expression of FRs on the surface of breast cancer cells is a strong predictor of poor outcome in patients with breast cancer (12, 41), and so we would anticipate that the SCP28 metastatic breast cancer cell line and the cell line from which it was created (MDA-MB-231) would express higher levels of FR than the M12 prostate cancer cell line.

Our experiments using Western and FACS confirm the variable expression of the FR in all of our cells, while the confocal immunocytochemistry further verifies the presence of FR on the cell surface in our tumor cell lines. While we unexpectedly show increased expression of FR in the BJ fibroblast cells, previous results using normal cell types indicate that FR expression is

luminal rather than on the cell surface. That said, additional experiments using FACS would confirm this and ultimately lend credence to our assertion that FR, while expressed in normal cells, would not be targeted by our TCRNs as FR expression is not on the surface of our cells. Additionally, we found that FR is a cell surface protein that is difficult to isolate without disrupting its confirmation, which is necessary for detection using our primary antibody. We attribute much of the background observed in our FR Westerns to dimerization or fragmentation of the FR protein or even FR complexing with other proteins. We plan to further confirm our results using other antibodies.

Our FACS and Western assays also independently confirm the expression of the PSMA protein in the M12 prostate cancer cell lines, which may, based on the literature (39), also be exploited to bring FA into cells. By inference, this protein will be able to complement the FR in transporting the FA tagged nanoparticples into the cell. Further characterization of the PSMA protein using confocal-based immunocytochemistry will be done to determine PSMA's ability to be targeted by our TCRNs.

To further strengthen all of our assays, we plan to repeat this characterization using M12 and MDA-231 cells that have been engineered to over-express FR or with cells expressing a dominant-negative mutant variant of the FR protein to reduce FR expression and function. Using these FR engineered cells, we can begin to more reliably track the movement of the TCRNs into the cells with confocal analysis, comparing high FR cells with cells that have either intermediate FR expression or low FR expression. If the TCRNs perform as expected, we expect to see a difference in the speed of dye uptake by the cells, as well as perhaps more clear evidence of nuclear deposition. We will then track the TCRN uptake using Live Cell Confocal Microscopy and record the timing of cellular uptake and association with the nucleus of the cell. To

maximize the expression of the FR on the cell surface, we can also grow cells for a period of time in FA deficient media, thereby allowing for more exposed, uncomplexed FR on the cell surface.

Our confocal experiments indicate that the Nile Red dye loaded FA-labeled TCRNs can be taken up by the cells and are able to associate with the nucleus while maintaining cell viability. Preliminary results suggest very little, if any, nuclear deposition of dye into the cells, yet there is significant association with the nucleus rather than just complete cytoplasmic distribution. To further confirm specific subcellular delivery of the dye rather than simple nuclear association of the dye/NPs, TCRNs have been designed to be tagged with Cy5 dye. This TCRN labeling, together with the Nile Red or DiR internally loaded dye, would allow tracking of the TCRN versus when and where the dye is released within the cell.

We find that the cells have a dose-dependent tolerance of the TCRNs, with optimal concentrations consistent with what translates into tolerable and detectable doses *in vivo*. Our results also show that cells do not survive well with higher concentrations of the TCRNs; yet our experiments do not distinguish between the effects of the TRCN, the dye, or the combination of dye and NP. To determine the relative contribution of each of these components we would need to repeat the cytotoxicity experiments to include treatments with 1) the dyes alone 2) the empty (dye free) TCRNs and 3) the dye loaded TCRNs without the FA moiety. Also, since the TCRNs are responsive to changes in pH, we plan to vary the pH to confirm this function and to investigate the influence pH has on the TCRN's ability to affect the cell at various concentrations.

We can also conclude from the *in vivo* experiments that the TCRNs can safely be administered to animals intravenously and that they retain their ability to deposit their contents in

tissues in an *in vivo* environment. We find that the TCRNs loaded with DiR are retained in the animal for up to 7 days without being excreted through typical channels with no association with the liver. We also observe tumor fluorescence using the SCP26 cells (luciferase), and after TCRN injection, there is only modest overlap of the DiR from the TCRN and the luciferase from the SCP26 cells. In the prostate cancer cells that were unlabeled (M12), we did find some overlap with the tumor in a few of our mice, suggesting that the colocalization of TCRN with tumor may be tumor-specific or that it could be dependent on the method and efficiency of injection (see below). While much more work needs to be done, our efforts open the possibility for further work with these NPs in future *in vivo* studies, providing more selective targeting after alteration of the TCRN structure.

Since the clinical relevance of the TCRNs hinges on their ability to specifically localize to the tumor tissue in live animals, we propose modifications of the *in vivo* component of our experiment. First, the selection of cells for the xenograft tumor is critical. We discovered that the SCP26 cells were over engineered with respect to their ability to express 2 kinds of luciferase and a GFP, and the knockdown of Smad4 in these cells is achieved by expression of a shRNA with GFP as selection marker, so the cells will constantly express GFP and thereby have green fluorescence (34). Even though the DiR dye has a spectrum that is sufficiently distinct from the GFP and we are able to specify filters that target the DiR, our cells may still produce background levels of fluorescence that may confound the results. Because of this, we plan to use cells that only express luciferase in addition to their increased expression of FR (MDA-MB-231-luciferase), so that we will be able to control the luciferase fluorescence with the addition of D-luciferin. This fluorescent signal would enable us to restrict our ROI to the tumor and reduce extraneous tissue that could dilute our signal. Our expectation is that this should enable us to see

a measurably stronger signal in the cells with a higher expression of FR compared to those that have their expression knocked down. To determine the precise location within the tumor, as well as within the tumor cells, we would further evaluate the deposition of TCRNs by employing confocal microscopy on the excised tumor tissue to detect both the dye from the TCRN and luciferase.

We found that the administration of the TCRNs intravenously was quite tedious for our *in vivo* studies. Since the Xenogen imaging chamber makes intravenous injections extremely difficult, we needed to find a protocol that permits injections to take place outside of the chamber in a more controlled environment to optimize success. This required us to eliminate the first post-treatment Xenogen reading (immediately post injection), which, based on our results, does not show much of a measureable difference in fluorescent signal in any of our experiments. The loss of this data point would not be as significant as the loss of animals incurred from rushed injections resulting from perivascular leakage of drug, which often occurred during our experiment. A clear intravenous injection also assures us that the dosage delivered is accurate and free from extravascular background signaling. Preliminary tests using either tail vein and/or retro-orbital injection methods both showed significant promise when done outside of the Xenogen staging area.

In addition, we found significant bleeding of signal from one animal to another adjacent animal as a result of high fluorescent signals from neighboring tumors. This confounded some results where some tumors showed much higher signals than was to be expected based on tumor size. Thus, shielding individual animal during imaging with a barrier divider will be done, which will prevent radiant signal from adjacent animals, a problem we encountered during our imaging.

Clearly, the ultimate confirmation of TCRN efficacy will come when the NPs are loaded with an actual chemotherapeutic agent and subjected to the same *in vitro* and *in vivo* experiments. These results, combined with our *in vitro* and *in vivo* preliminary data, will allow correlation of cytotoxicity and tumor burden reduction with drug concentration, while additional experiments using cells with alterations in FR expression will prove the importance of direct tumor cell targeting in a living system.

In conclusion, despite a lack of specific nuclear deposition of TCRN contents in tumor cells, our data are quite encouraging and suggest that the TCRNs have the potential to target tumor cells using the FR and that the TCRNs are stable *in vitro* and *in vivo*. By refining and expanding our *in vitro* experiments, we will be able to exercise greater control over all of these variables in future experiments, translating these *in vitro* results to more definitive results *in vivo* in order to determine the value of TCRNs in a therapeutic setting. In the end, if we can only demonstrate nuclear association and not delivery, this finding would still be significant and would suggest needed alteration in the TCRN to trigger nuclear delivery. Targeting FR-expressing carcinoma cells and focusing drug delivery to the nucleus will ultimately result in greater efficacy with lower drug concentrations, especially with therapeutic compounds that target and damage DNA as their mode of action.

Chapter 5

References

1. U.S. Department of Health and Human Services CfDCaPaNCIAawcgu. U.S. Cancer Statistics Working Group. United States Cancer Statistics: 1999–2006 Incidence and Mortality Web-based Report :. Atlanta; 2010 [updated 2010; cited 2010 10/18/2010]; Available from: http://apps.nccd.cdc.gov/uscs/toptencancers.aspx.
2. Weinberg RA. The biology of cancer. New York: Garland Science; 2007.
3. Peppas N, Hilt J, Thomas J. Nanotechnology in Therapeutics: Current Technology and Applications. Horizon Bioscience. 2007.
4. Hattori Y, Maitani Y. Folate-linked nanoparticle-mediated suicide gene therapy in human prostate cancer and nasopharyngeal cancer with herpes simplex virus thymidine kinase. Cancer Gene Ther. 2005;12(10):796-809.
5. Maeng JH, Lee DH, Jung KH, Bae YH, Park IS, Jeong S, et al. Multifunctional doxorubicin loaded superparamagnetic iron oxide nanoparticles for chemotherapy and magnetic resonance imaging in liver cancer. Biomaterials. 2010;31(18):4995-5006.
6. Faraji AH, Wipf P. Nanoparticles in cellular drug delivery. Bioorg Med Chem. 2009;17(8):2950-62.
7. Koo OM, Rubinstein I, Onyuksel H. Role of nanotechnology in targeted drug delivery and imaging: a concise review. Nanomedicine. 2005;1(3):193-212.
8. Cho WS, Cho M, Jeong J, Choi M, Han BS, Shin HS, et al. Size-dependent tissue kinetics of PEG-coated gold nanoparticles. Toxicol Appl Pharmacol. 2010;245(1):116-23.
9. Cho M, Cho WS, Choi M, Kim SJ, Han BS, Kim SH, et al. The impact of size on tissue distribution and elimination by single intravenous injection of silica nanoparticles. Toxicol Lett. 2009;189(3):177-83.
10. Malam Y, Loizidou M, Seifalian AM. Liposomes and nanoparticles: nanosized vehicles for drug delivery in cancer. Trends Pharmacol Sci. 2009;30(11):592-9.

11. Xu P, Van Kirk EA, Zhan Y, Murdoch WJ, Radosz M, Shen Y. Targeted charge-reversal nanoparticles for nuclear drug delivery. Angew Chem Int Ed Engl. 2007;46(26):4999-5002.
12. Meier R, Henning TD, Boddington S, Tavri S, Arora S, Piontek G, et al. Breast cancers: MR imaging of folate-receptor expression with the folate-specific nanoparticle P1133. Radiology. 2010;255(2):527-35.
13. Davis ME, Zuckerman JE, Choi CH, Seligson D, Tolcher A, Alabi CA, et al. Evidence of RNAi in humans from systemically administered siRNA via targeted nanoparticles. Nature. 2010;464(7291):1067-70. PMCID: 2855406.
14. Yamada K, Yamamoto N, Yamada Y, Mukohara T, Minami H, Tamura T. Phase I and pharmacokinetic study of ABI-007, albumin-bound paclitaxel, administered every 3 weeks in Japanese patients with solid tumors. Jpn J Clin Oncol. 2010;40(5):404-11. PMCID: 2862657.
15. Majoros IJ, Williams CR, Becker A, Baker JR, Jr. Methotrexate delivery via folate targeted dendrimer-based nanotherapeutic platform. Wiley Interdiscip Rev Nanomed Nanobiotechnol. 2009;1(5):502-10. PMCID: 2944777.
16. Salata O. Nanotechnology in Therapeutics: hydrogels and beyond. Journal of Nanobiotechnology. 2007;5(1):5.
17. Xu P, Li SY, Li Q, Van Kirk EA, Ren J, Murdoch WJ, et al. Virion-mimicking nanocapsules from pH-controlled hierarchical self-assembly for gene delivery. Angew Chem Int Ed Engl. 2008;47(7):1260-4.
18. Xia W, Low PS. Folate-targeted therapies for cancer. J Med Chem. 2010;53(19):6811-24.
19. Shen LX, Cook C, Fitzloff JF. Comparison of the stereoselective metabolism of propranolol and metoprolol using cDNA expressed human CYP450 isozymes. Drug Metab Rev. 2003;35:185-.
20. Doucette MM, Stevens VL. Folate receptor function is regulated in response to different cellular growth rates in cultured mammalian cells. J Nutr. 2001;131(11):2819-25.
21. Okarvi SM, Jammaz IA. Preparation and *in vitro* and *in vivo* evaluation of technetium-99m-labeled folate and methotrexate conjugates as tumor imaging agents. Cancer Biother Radiopharm. 2006;21(1):49-60.

22. Iwakiri S, Sonobe M, Nagai S, Hirata T, Wada H, Miyahara R. Expression status of folate receptor alpha is significantly correlated with prognosis in non-small-cell lung cancers. Ann Surg Oncol. 2008;15(3):889-99.
23. Chen H, Ahn R, Van den Bossche J, Thompson DH, O'Halloran TV. Folate-mediated intracellular drug delivery increases the anticancer efficacy of nanoparticulate formulation of arsenic trioxide. Mol Cancer Ther. 2009;8(7):1955-63.
24. Parker N, Turk MJ, Westrick E, Lewis JD, Low PS, Leamon CP. Folate receptor expression in carcinomas and normal tissues determined by a quantitative radioligand binding assay. Anal Biochem. 2005;338(2):284-93.
25. Pietrzik K, Bailey L, Shane B. Folic acid and L-5-methyltetrahydrofolate: comparison of clinical pharmacokinetics and pharmacodynamics. Clin Pharmacokinet. 2010;49(8):535-48.
26. Henderson GB. Folate-binding proteins. Annu Rev Nutr. 1990;10:319-35.
27. Salazar MD, Ratnam M. The folate receptor: what does it promise in tissue-targeted therapeutics? Cancer Metastasis Rev. 2007;26(1):141-52.
28. Ke CY, Mathias CJ, Green MA. The folate receptor as a molecular target for tumor-selective radionuclide delivery. Nucl Med Biol. 2003;30(8):811-7.
29. Hickson J. *In vivo* optical imaging: preclinical applications and considerations. Urol Oncol. 2009;27(3):295-7.
30. Lyons SK. Advances in imaging mouse tumour models *in vivo*. J Pathol. 2005;205(2):194-205.
31. Amos WB, White JG. How the confocal laser scanning microscope entered biological research. Biol Cell. 2003;95(6):335-42.
32. Community IVI. Are you new to *in vivo* imaging? : *In vivo* Imaging Community 2010 [updated 2010; cited 2010 10/10/2010]; Available from: http://invivoimagingcommunity.com/in_vivo_imaging_modalities_1 http://invivoimagingcommunity.com/in_vivo_imaging_modalities_2.
33. Bae VL, Jackson-Cook CK, Maygarden SJ, Plymate SR, Chen J, Ware JL. Metastatic sublines of an SV40 large T antigen immortalized human prostate epithelial cell line. Prostate. 1998;34(4):275-82.

34. Korpal M, Yan J, Lu X, Xu S, Lerit DA, Kang Y. Imaging transforming growth factor-beta signaling dynamics and therapeutic response in breast cancer bone metastasis. Nat Med. 2009;15(8):960-6.
35. Kalchenko V, Shivtiel S, Malina V, Lapid K, Haramati S, Lapidot T, et al. Use of lipophilic near-infrared dye in whole-body optical imaging of hematopoietic cell homing. J Biomed Opt. 2006;11(5):050507.
36. Quartzy. 1,1'-dioctadecyl-3,3,3',3'-tetramethylindotricarbocyanine iodide ('DiR'; DiIC18(7)). [cited 2010]; Search through names, research, skills, publications and more...]. Available from: https://www.quartzy.com/reagentdetail/334594.
37. Fowler SD, Greenspan P. Application of Nile red, a fluorescent hydrophobic probe, for the detection of neutral lipid deposits in tissue sections: comparison with oil red O. J Histochem Cytochem. 1985;33(8):833-6.
38. Givan AL. Flow cytometry : first principles. 2nd ed. New York: Wiley-Liss; 2001.
39. Yao V, Berkman CE, Choi JK, O'Keefe DS, Bacich DJ. Expression of prostate-specific membrane antigen (PSMA), increases cell folate uptake and proliferation and suggests a novel role for PSMA in the uptake of the non-polyglutamated folate, folic acid. Prostate. 2010;70(3):305-16.
40. Hrapkiewicz K, Medina L, Holmes DD. Clinical laboratory animal medicine : an introduction. 3rd ed. Ames, Iowa: Blackwell Pub.; 2007.
41. Hartmann LC, Keeney GL, Lingle WL, Christianson TJ, Varghese B, Hillman D, et al. Folate receptor overexpression is associated with poor outcome in breast cancer. Int J Cancer. 2007;121(5):938-42.

Vita

Mario Dance was born in Yokohama Japan on the Yokuska Naval Base, as a Citizen of the USA. He received his BS in Biochemistry/Nutrition from Virginia Polytechnic Institute and State University in 1986 and his DVM from Virginia-Maryland Regional College of Veterinary Medicine in 1990. During his undergraduate years, he participated in research at the Patuxent Wildlife Research Station in Laurel, MD, and did an undergraduate research project with the Department of Biology at VPI&SU. While in veterinary school he did a rotation at the Centers for Disease Control. After graduating from veterinary school he worked for 5 years in private practice before coming back to research, initially in the Department of Pharmacology and Toxicology at VCU and ending in the Division of Animal Resources at VCU.